CHAPTER 4

Active Microwave Sensing of the Atmosphere

Active Microwave Working Group

Atmosphere Panel:

WILLIAM R. BANDEEN, *Cochairman*
ISADORE KATZ, *Cochairman*

David Atlas
Gordon A. Beals
Charles W. Bostian
Thomas A. Croft
Richard J. Doviak
Roger M. Lhermitte
Hans J. Liebe
Gordon E. Peckham
Allan C. Schell
Paul L. Smith, Jr.
Robert A. Stokes
Richard R. Weiss
Raymond Wexler
Carl A. Wiley

The meteorological satellite program is now in its 15th year. Beginning with the launch of Tiros 1 on April 1, 1960, 18 experimental Tiros, Nimbus, and geostationary Applications Technology Satellite (ATS) satellites carrying meteorological instruments have been launched. Research with early television pictures led to many discoveries concerning the organization and movement of cloud patterns and their relationship to meteorological processes; limited operational use of television pictures in weather forecasting began soon after the launch of Tiros 1. Subsequent experimental satellites carried omnidirectional and multichannel scanning radiometers. The radiometer data were applied in many different ways, including studies of radiation balance, mapping of cloud cover, tracking of storms, determination of surface temperatures and cloud-top heights, inference of mean tropospheric water vapor content, and global mapping of mean stratospheric temperature.

The first geostationary satellite to carry a meteorological instrument (a spin scan cloud camera) was ATS–1, launched on December 7, 1966. Time-lapse "movies," made from images of the planetary disk taken approximately every 20 min from an altitude of 26 000 km, showed dramatically the short-term weather motions from space. New knowledge of wind, circulation, and wave features deduced from cloud motions; of interhemispheric mass transport; and of mesoscale systems (such as squall lines, tornadoes, and other severe weather) was acquired. The development of a technique to determine winds by tracking clouds was of major importance, and wind data determined from ATS–3, after more than 6 yr in orbit, are used operationally by the National Oceanic and Atmospheric Administration (NOAA).

Nimbus 3, launched in April 1969, departed markedly from its predecessors by carrying three new classes of experiments. The first experiment class, the monitor of

ultraviolet solar energy (MUSE), monitored wavelengths affected by the photochemical processes associated with the generation and destruction of ozone. A second experiment class, the interrogation, recording, and location system (IRLS), demonstrated the feasibility of locating moving platforms (such as balloons and buoys), collecting in situ measurements from them, and determining atmospheric winds and ocean currents from their movements. The third experiment class, the satellite infrared interferometer spectrometer (IRIS), which also provided global measurements of stratospheric ozone, was perhaps most dramatic in demonstrating the ability to remotely sense vertical profiles of temperature in the atmosphere. This ability was accomplished by suitably "inverting" spectral radiances measured over the 15-μm absorption band of CO_2. The success was so dramatic that vertical profiles from the satellite infrared spectrometer (SIRS) on Nimbus 3 and 4 were used operationally by NOAA from May 1969 to November 1972 when they were replaced by soundings from a new vertical temperature profile radiometer (VTPR) on the NOAA–2 operational satellite.

Many of the spacecraft and instrument technology and data applications techniques are used in the operational satellite system after they are tested and proved on experimental satellites. The previously mentioned evolution of vertical sounders from SIRS on Nimbus 3 and 4 to VTPR on NOAA–2 is a good example. The first Tiros operational satellite (TOS), Environmental Sciences Service Administration 1 (ESSA–1), was launched in February 1966. The first second-generation improved TOS (ITOS–1) was launched in January 1970. To date, 14 operational satellites (and prototypes) have been successfully launched.

Nimbus 5, which was launched on December 11, 1972, carried for the first time radiometers sensing emission in the microwave region of the spectrum. Data from a single-channel electrically scanning microwave radiometer (ESMR) have demonstrated the potential of the measurement for mapping sea ice through clouds and for delineating precipitating cloud systems over the oceans of the world. Data from the Nimbus 5 microwave sounder (NEMS) have shown the ability of the NEMS to sound atmospheric temperature through cloudiness. The addition of microwave channels to infrared sounders of the future will markedly improve their accuracy and utility.

Skylab, launched in May 1973, carried numerous experiments for Earth observations, including a multispectral camera, an infrared spectrometer, a multispectral scanner, and a composite active/passive microwave system. Although these experiments were designed primarily for Earth resources survey and oceanography, of particular interest to the atmosphere panel is the active/passive radiometer/scatterometer (RADSCAT)/altimeter system, designed to measure ocean-surface characteristics (such as roughness) from which surface winds may be inferred. This experiment is mentioned in chapter 3 and discussed further in chapter 5.

The first Synchronous Meteorological Satellite (SMS) carrying a two-channel visible and infrared spin scan radiometer (VISSR), which is the prototype of the Geostationary Operational Environmental Satellite (GOES) soon to be placed in service by NOAA, was launched on May 17, 1974. The SMS provides, for the first time, continuous viewing of weather features, both day and night; it also collects and relays environmental data from remote platforms such as buoys, ships, and automatic stations. Also, the ATS–6—NASA's first three-axis-stabilized geostationary satellite carrying an advanced two-channel (visible and 11-μm infrared) radiometer—was launched on May 30, 1974, and is operating successfully.

Nimbus 6 carries eight sensors, including advanced atmospheric sounders, radiometers, and a data collection and platform location system. Of particular interest are the two passive microwave instruments. One instrument, an advanced ESMR, has a single spectral band (37 GHz; wavelength λ of 0.81 cm) with dual polarization, a conical scan, and an

instantaneous field of view (IFOV) of 25 km. The other instrument, the scanning and microwave sounder (SCAMS), will map tropospheric temperature profiles, water vapor abundance, and cloud-water content. It will sense radiation in the 60-GHz (O_2) absorption region, the 22-GHz water vapor absorption region, and the 31-GHz window region of the spectrum.

The evolution of meteorological satellites is illustrated in figure 4–1, in which the satellite and the date of the first launch for each series (except Skylab) is shown. Nimbus-G, SEASAT–A, Space Shuttle, and Tiros-N are approved future missions. The Earth Observatory Satellite (EOS) and the Synchronous Earth Observatory Satellite (SEOS) are only concepts; they are shown merely to illustrate possible types of future missions.

Tiros-N will carry an advanced atmospheric sounder (including both infrared and passive microwave channels), an advanced radiometer imaging in the visible and infrared, and an advanced data collection and platform location system. Nimbus-G (to be launched in 1978) is scheduled to carry the following nine instruments: (1) scanning multichannel microwave radiometer (SMMR), (2) coastal zone color scanner (CZCS), (3) solar and backscattered ultraviolet and total ozone mapping system (SBUV/TOMS), (4) Earth radiation budget (ERB), (5) lower atmospheric composition and temperature experiment (LACATE), (6) stratospheric and mesospheric sounder (SAMS), (7) stratospheric aerosol measurement (SAM II), (8) measurement of air pollution from satellites (MAPS), and (9) temperature humidity infrared radiometer (THIR). Of particular interest to the atmosphere panel is the SMMR. The payload for SEASAT–A (to be launched in 1978) has not been officially determined, but a tentative payload, including several active microwave instruments, includes the following:

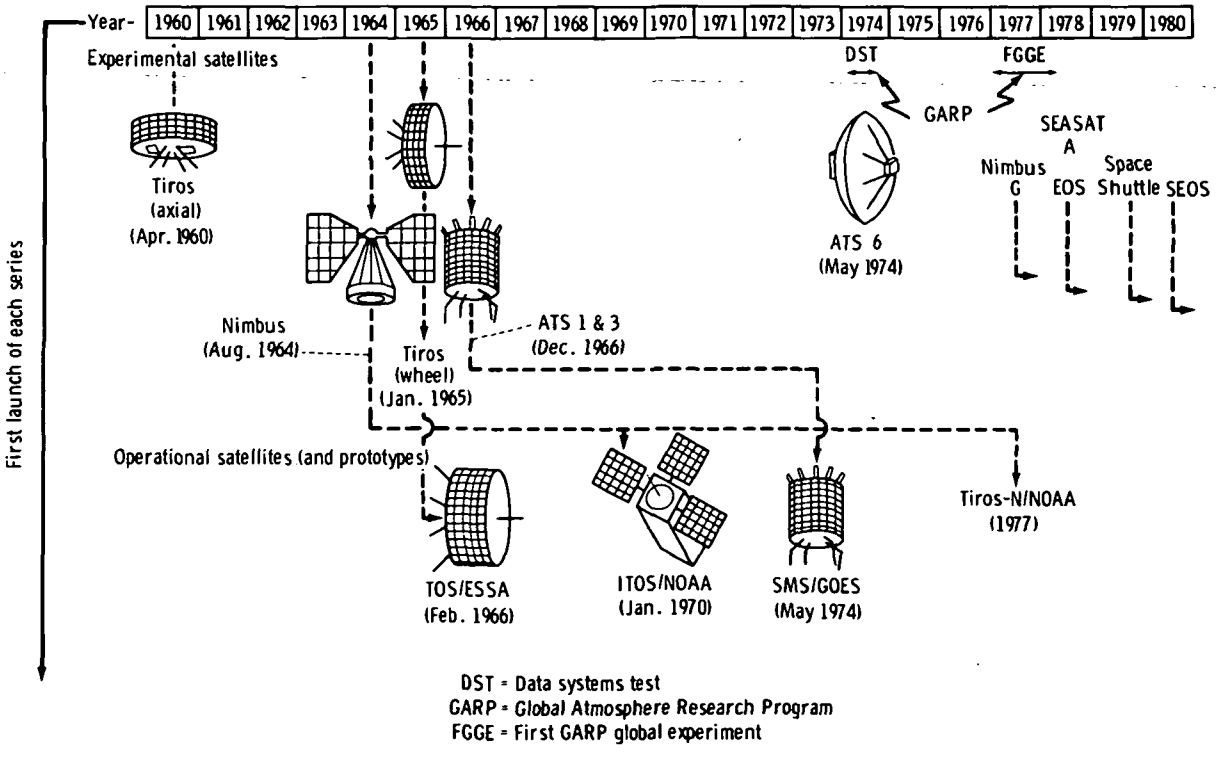

FIGURE 4–1.—Evolution of meteorological satellites (and other satellites with meteorological instruments).

(1) SMMR, (2) fan beam scatterometer (FBS), (3) radar altimeter (RA), (4) visible and infrared radiometer (VIR), and (5) synthetic aperture radar (SAR) or wave directional spectrometer (WDS).

DISCIPLINE OBJECTIVES IN THE ATMOSPHERIC SCIENCES

The decade of the 1960's saw the development of a comprehensive meteorological satellite program, with a concomitant increase in capabilities for useful application on a scale previously impossible. In the early 1970's, environmental problems came forcefully to public attention. Presently, a unique combination of opportunities and challenges exists—a new capacity for useful applications to the needs of society at a time when the influence of public opinion provides a driving force toward solutions for pressing problems. These circumstances are likely to have far-reaching influences on the development of atmospheric sciences in the coming years. A recent report prepared by the Committee on Atmospheric Sciences of the National Research Council, National Academy of Sciences (ref. 4–1), lists four meteorological objectives that can contribute most to the solution of pressing problems in the 1970's.

1. Weather prediction: To extend the capability for useful predictions of the weather and atmospheric processes

2. Atmospheric pollution: To contribute to the development of the capability to manage and control the concentrations of air pollutants

3. Climate and weather modification: To establish mechanisms for rational examination of deliberate and inadvertent means for modifying weather and climate

4. Weather danger and disaster warning: To reduce substantial human casualties, economic losses, and social dislocations caused by weather

The six NASA meteorology program objectives are as follows. (Objectives 2 to 5 correspond to the four meteorological objectives of the Committee on Atmospheric Sciences.)

1. Operational support: Support the development of the operational meteorological satellite system.

2. Weather prediction: Develop space technology for determining the vertical structure of the atmosphere globally, which, when supplemented by simulation techniques, models, and conventional observations, will provide required data with emphasis on large-scale long-term weather forecasts.

3. Atmospheric pollution: Develop a space-sensing capability to identify and quantitatively monitor the distribution of natural and manmade pollution in the lower and upper atmosphere on global and regional scales.

4. Climate and weather modification: Apply space-acquired data from remote sensors, data collection systems, and/or in-flight experiments requiring unique orbital conditions (such as a gravity-free environment) to the development of models and the establishment of mechanisms for the rational examination of deliberate and inadvertent means for modifying weather and climate.

5. Weather danger and disaster warning: Develop and establish a system for continuous observation of atmospheric features to permit early identification and quantitative measurement of atmospheric conditions conducive to the formation of severe atmospheric phenomena (e.g., thunderstorms, tornadoes, hurricanes, etc.) and to serve as a basis for timely warning to the public.

6. Processes and interactions: Investigate fundamental atmospheric processes and interactions on various temporal and spatial scales (within the atmosphere, in response to solar inputs, and at the air-surface interface) through the observation of the structure, composition, and energetics of the atmosphere for the purpose of effectively applying space capabilities in pursuance of the previously mentioned objectives.

The scientific and meteorological communities of the world, represented by the International Council of Scientific Unions (ICSU) and the World Meteorological Organization (WMO), have defined and undertaken an

ambitious and extensive international research program, the GARP. The Joint Organizing Committee (JOC) for GARP has been formed by these two organizations to provide leadership and direction to this program. At the first meeting in April 1968, the JOC provided the following definition and objectives for GARP:

> A program for studying those physical processes in the troposphere and stratosphere that are essential for an understanding of the transient behavior of the atmosphere as manifested in the large scale fluctuations which control changes of the weather; this would lead to increasing the accuracy of forecasting over periods from one day to several weeks, and the factors that determine the statistical properties of the general circulation of the atmosphere could lead to better understanding of the physical basis of climate.

Those objectives are closely analogous to objectives 2 (weather prediction) and 4 (climate and weather modification) of the NASA meteorological program.

The GARP has expanded rapidly, and it now involves a series of interrelated theoretical and observational subprograms. The GARP Atlantic tropical experiment (GATE) and the FGGE scheduled for 1977 to 1978 are particularly noteworthy. Also, a DST was conducted during 1974 to test elements of FGGE in preparation for the complete experiment (fig. 4–1).

The FGGE in intended to provide detailed measurements of the large-scale state and motions of the entire atmosphere over a period of a year or more (1977 to 1978). The main objectives of FGGE (ref. 4–2) are directed at developing more realistic numerical models of the atmosphere, assessing the ultimate limits of weather predictability, and designing appropriate weather observing systems for prediction of the large-scale features of the general circulation.

The basic data requirements for FGGE have been defined by JOC and are summarized in table 4–I. In addition to these parameters, an auxiliary list of desirable parameters has been defined. These additional requirements are soil moisture; reflected, scattered, and emitted radiation; albedo and radiation balance; snow and ice cover; cloud cover (and type); precipitation areas; ozone; and ocean temperature above the seasonal thermocline.

Because of the development time required, it is not practical to consider an orbiting radar to support FGGE in the period 1977 to 1978. The purpose of this discussion of GARP is to present briefly the scope of a major ongoing international effort that is in accord with several of the meteorological objectives of NASA and the National Academy of Sciences. In this framework, it is not

TABLE 4–I.—*The JOC Data Requirements for FGGE* [a]

Basic parameters	Horizontal resolution, km	Vertical resolution		Accuracy
		Troposphere	Stratosphere	
Mid and high altitudes				
Temperature	500	4 levels	3 levels	±1 K
Wind	500	4 levels	3 levels	±3 m/sec
Relative humidity	500	2 degrees of freedom	.....	±30 percent
Sea surface temperature	500	.....	.....	±1 K
Pressure (reference level)	500	.....	.....	±0.3 percent
Low altitudes				
Temperature	500	4 levels	3 levels	±1 K
Wind	500	4 levels	3 levels	±2 m/sec
Relative humidity	500	2 degrees of freedom	.....	±30 percent
Sea surface temperature	500	.....	.....	±1 K

[a] One measurement per day is required; 2 per day are desirable.

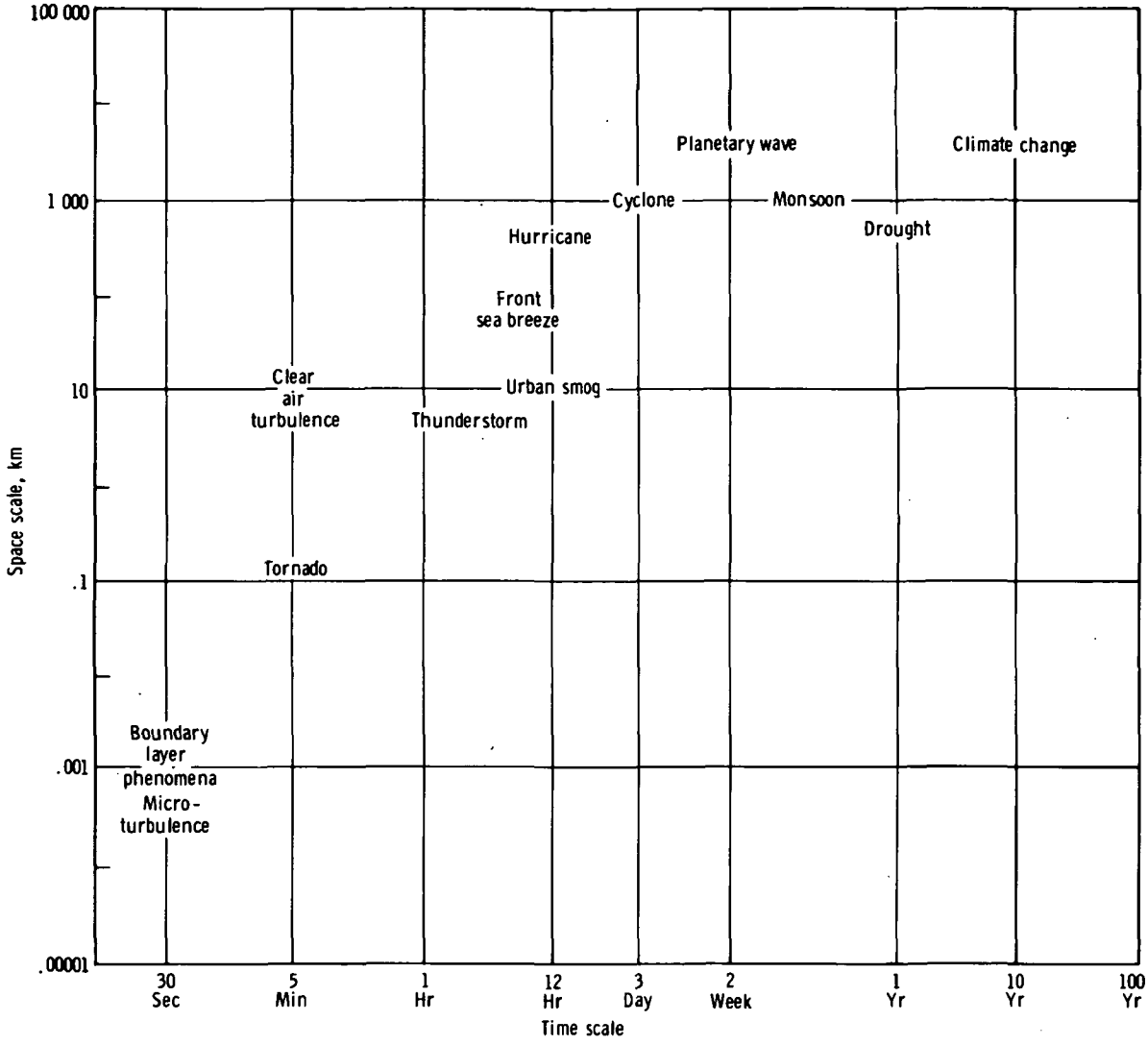

FIGURE 4–2.—Time and space scales of meteorological phenomena.

unreasonable to contemplate an active microwave system that could contribute to the success of a similar program in the future.

The FGGE is concerned primarily with atmospheric phenomena having time scales of approximately a week or longer. However, many important meteorological phenomena have shorter time scales, some of which are illustrated in figure 4–2. With reference to the NASA meteorology program objectives and figure 4–2, the geostationary satellite is peculiarly applicable to program objective 5 (weather danger and disaster warning), which involves phenomena having time scales less than 12 hr. The idea of orbiting an active microwave system at the geostationary altitude (36 000 km) has indeed seemed well beyond serious consideration in the past. However, with the approach of the Space Shuttle era and in terms of the tremendous technological advances of the past decade and of those advances that will surely come in the future, it seems appropriate to assess again the possible applications to the atmospheric sciences of active microwave systems in either near-Earth or geostationary orbits.

PART A

MEASUREMENT TECHNIQUES AND PRINCIPAL APPLICATION AREAS

APPLICATIONS OF CONVENTIONAL PULSE RADAR SYSTEMS TO METEOROLOGICAL OBSERVATIONS

Radars have been used for meteorological observations since shortly after the development of centimetric radar equipment in the early 1940's. The history of the meteorological uses of radar can be traced in references 4–3 to 4–13. In addition, the proceedings or preprint volumes from the series of radar meteorology conferences (formerly called weather radar conferences), published by the American Meteorological Society, provide an excellent history of the development and application of radar technology in meteorology.

The most important aspect of radar for meteorological observations is its ability to observe precipitation at distances up to several hundred kilometers, which makes it a true remote sensor for meteorological applications. Ground-based weather radars have been useful mainly for subsynoptic scale, or "mesoscale," observations. They readily provide observations with space continuity impossible to attain with the ordinary synoptic weather-reporting network. Such radar observations are of enormous value in a wide variety of applications, including short-term forecasting for local areas or terminal points and for many research investigations.

However, to extend the value of weather radar observations to the synoptic scale remains difficult. The area covered by a single ground-based weather radar set is too small to encompass most synoptic-scale features of interest, and techniques for meshing observations from numerous radar installations to provide coverage of larger areas are only now being developed. The so-called "Ligda montages" (ref. 4–14), which were synthesized from the observations of many radar systems located at different sites, were the first attempt to assemble data from several radars, thus providing examples of how synoptic-scale patterns can be discerned in radar observations. The development of automated techniques for meshing such observations is one objective of the NOAA digitized radar experiments (D/RADEX) program now in progress (ref. 4–15).

Weather radar observations are of value in forecasting for periods of up to 6 hr. A limiting factor is the variability of precipitation in space and time; the plan-position-indicator (PPI) scope of a weather radar set operating during a typical summer afternoon of convective activity reveals a process of continuous evolution. Cells and storm systems grow and decay. Old cells disappear from the scope and new ones form; sometimes cells merge, and less frequently they even split. It is even difficult to define a "cell" or "storm" or "echo" in an objective way, although there have been recent developments in this direction (ref. 4–16). These conditions greatly inhibit the use of radar observations of precipitation for forecast purposes, when extrapolation over appreciable intervals of space or time is required.

Hydrology is another important area in which weather radar is finding increasing application. Weather radar observations are ideally suited for such tasks as mapping accumulated precipitation amounts over specific watershed areas, particularly when short time intervals are involved (as in the case of flash-flood situations). This application places stringent demands on making accurate quantitative measurements of echo intensities with radar systems that are calibrated accurately. Even then, the problem of relating the radar measurements to precipitation rates and amounts has yet to be completely solved.

Characteristics of Ordinary Pulse Weather Radars

Weather radar observations provide a variety of information concerning the precipitation responsible for the echoes. This

information can be divided into two categories, according to whether it can be extracted from single "snapshot" observations (for example, single PPI scans) or whether repetitive observations over an interval of some minutes or hours are required. Such categorization may be helpful in evaluating the potential use of satellites as weather radar platforms because orbiting satellites provide primarily a "snapshot" capability. Obtaining repetitive radar observations in most instances requires operating from geosynchronous satellites or a system of multiple satellites.

The "snapshot" category of information includes the observation of the location, size, and shape of the precipitation regions from two- or three-dimensional imagery. Also, the precipitation structure can be determined from the pattern of the echoes and the "texture" of individual echo elements, and the intensity and intensity gradients can be determined from relative or absolute measurements of echo intensity. These characteristics are usually adequate to deduce the basic nature of the precipitation process; for example, stratiform compared to convective, airmass compared to squall line, etc. That information, together with synoptic information such as environmental wind data and the characteristics of the airmass, can be used to develop short-term forecasts of the future behavior of the precipitation in the area surveyed by the radar. However, the typical rapid evolution of the precipitation restricts the time period of validity of any such forecasts.

The situation can be improved somewhat by making repetitive observations over a period of time. They yield a second category of information, which is related to the movement (speed and direction) and time evolution or to persistence (duration) of the precipitation regions. The situation, with respect to repetitive observations, is seldom as clear-cut as it might at first appear. For example, even with echo patterns having fairly well defined cellular elements, it typically takes more than 15 min to establish reasonably good estimates of cell movements. However, the lifetimes of convective cells are often on the order of 30 min, and new cells have a tendency to develop alongside old ones, so that movement and evolution interact in a complicated way. Moreover, the direction of cell movement is usually different from that of the storm system as a whole.

The essential conclusion is that, although "snapshot" radar observations provide useful information about the space distribution of precipitation at a given time, repetitive observations are still necessary in most operational applications such as forecasting. Even so, the length of time over which the observations can be extrapolated to develop the forecasts is typically rather short. There remains the prospect that this time might be extended by developing numerical weather prediction models using current and past precipitation data as input, thus providing forecasts of the future course of development of the precipitation.

The observational capabilities of weather radar may possibly be extended by adding Doppler, multiple polarization, and/or multiple wavelength features to the radar system. The merits of adding these features are discussed in other sections of this chapter.

In the usual ground-based weather radar applications, the choice of radar wavelength is determined mainly by a compromise between the difficulties caused by attenuation (as the wavelength decreases below 10 cm) and the expense of obtaining the desired angular resolution (beamwidth) at long wavelengths. Research radars can operate at 10-cm wavelengths to virtually remove attenuation difficulties and can accept the increased expense required to obtain good beamwidth resolution. Operational radars tend to be designed for the 10-, 5-, or sometimes even the 3-cm wavelength regions. For a fixed beamwidth, the variations in available transmitter power and receiver sensitivity generally serve to keep the overall system sensitivity (in terms of minimum detectable radar reflectivity factor) over this range of wavelengths approximately inde-

pendent of the selected wavelength. Airborne weather radars generally operate at 5- or 3-cm (or even shorter) wavelengths to take advantage of the smaller sizes of the equipment.

The antenna beamwidths ordinarily used in weather radars range from approximately 1° to 3°, although there are exceptions beyond these limits in both directions. The narrower beamwidths are usually found in research weather radar systems. A lower bound near 1° is set even for these radar systems by some combination of tradeoff relative to (1) the huge antennas needed to reduce the beamwidths below 1°, (2) the increased scanning time required (because the number of angular elements to be scanned increases in proportion to the inverse of the product of the beamwidths), and (3) the increased amounts of data (from the greater number of angular elements) that have to be handled. For many purposes, good vertical resolution is more important than good horizontal resolution, so there can be advantages in using height-finder-type antennas.

Operational network weather radars typically have somewhat larger beamwidths. For example, the U.S. Air Force FPS–77 has a beamwidth of approximately 1.6°, whereas the National Weather Service WSR–57 has a beamwidth of approximately 2.2°. Beamwidths of 3° or larger are found only in airborne weather radars and in a few other radars in which the primary use involves relatively short-range observations.

The other characteristics of weather radars are generally governed by various practical considerations. Usually, values of peak power and pulse duration are comfortably within the state of the art, there seldom being any real requirement, when observing precipitation, to press for the relatively modest improvements in sensitivity that might be obtained by pushing those values toward the state-of-the-art limits. Upper limits on the pulse repetition frequency (PRF) are related to considerations of maximum unambiguous range and to the fact that precipitation echoes have pulse-to-pulse time correlations up to 5 to 20 msec (at $\lambda = 10$ cm); thus, little can be gained in the assessment of echo mean intensity by increasing the PRF beyond a certain value.

Weather Radar Observations From Orbiting Satellite Platforms

It is only natural to ask whether it is possible to combine the capabilities of radar observation of weather with the advantages offered by a satellite platform. Orbiting satellite platforms would provide the potential for a significant increase of the radar coverage to the synoptic scale, as well as extending observations to the remote oceans and other areas that are not presently covered by any weather radar system. Another advantage of the satellite platform is a possible use of shorter wavelengths because the radar signals do not have to traverse long paths through rain, thereby reducing the importance of attenuation.

The idea of installing a weather radar on a satellite was considered even before the first Tiros satellite went into orbit (refs. 4–17 to 4–21). Radars, however, require heavy transmitters and large amounts of prime power; therefore, they were not well suited to the early satellite technology. The amount of weight and power that can be carried in space has increased. It is therefore appropriate to reconsider the practicality of satellite-borne radars and the nature of the meteorological information that could be obtained with them.

Dennis (refs. 4–22 and 4–23) reviewed the early proposals and discussions of satellite weather radars and concluded that weather radar observations from an orbiting satellite would be of little meteorological value. He noted two basic problems in the use of satellite-borne radar systems:

1. The need for separating the contributions of the precipitation and of the ground or sea surface underneath to the echoes limits the radar observations to a narrow subsatellite swath. He suggested that the swath width might be smaller than 40 km. This limitation can be overcome by using tech-

niques that permit separating the ground and precipitation contributions to the echoes.

2. As previously noted, radar observations of precipitation cannot be extrapolated very far in either time or space. An orbiting satellite providing observations on a 12- or 24-hr return cycle would therefore be of little value to the usual operational applications of weather radar data, such as mesoscale analysis and forecasting. However, this problem only tends to restrict the effective application of satellite weather radar observations to the monitoring of precipitation in longer, persistent meteorological systems such as hurricanes.

Dennis' findings essentially halted serious consideration of satellite-borne weather radars. A 1969 report (ref. 4–24) included only a brief mention of the use of satellite radars for precipitation measurements. Although the material in this report outlines only possible solutions and there are few specific details, its tone is quite optimistic. It is mentioned that an average power of 20 W would still be adequate for a radar installed aboard a synchronous satellite. The radar would operate at a wavelength of 2 cm, use a 10-m-size antenna, have a range resolution of 75 km, and have an azimuth resolution of 150 km. Such a radar should be capable of detecting rain extending 1 km in height with a rainfall rate greater than 10 mm/hr.

A textbook of radar meteorology, authored by V. D. Stepanenko (ref. 4–12), devotes a chapter to the use of radar and microwave radiometry in satellites for obtaining meteorological and hydrological information. A translation of textbook section 9.6, "Features and Effectiveness of the Detection of Clouds and Rain With Pulse Radar From Satellites," is included as appendix 4A to this chapter. He considers radars with both a downward-looking scanning pencil beam and a fixed planar (fan) beam.

As an example of the scanning pencil-beam system, he considers an X-band (λ=3 cm) radar in a satellite at an altitude of 400 km. The scanning angle is 78°. The beamwidth in the along-track dimension is 3.5°; in the across-track dimension, it is 0.51°. The PRF is 1150 Hz; and, with a peak power of 300 kW and a pulse duration of 1 μsec, the satellite can detect a rainfall rate of 1.5 mm/hr. Four satellites are supposed to be required. The author implies that, with the scanning narrow-pencil-beam radiation pattern, the effect of Earth echo is not important.

Earth echo is noted by Stepanenko to be important when a fixed planar beam is used. This type of antenna is considered mainly because it is simpler to construct than a scanning pencil-beam antenna and because it also allows the necessary minimum number of pulses on target to be readily obtained. Coverage of the Earth surface is obtained with two fixed antennas oriented perpendicular to the orbit plane of the satellite. (Although not stated explicitly, it is presumed that the antennas point to opposite sides of the satellite.) When the altitude is 400 km, a common receiver/transmitter is switched between the two antennas at a rate of 16 Hz. The width of the radiation pattern is 30° in the direction perpendicular to the groundtrack and 0.23° in the direction along the groundtrack. The peak power is 300 kW, and the pulse duration is 5 μsec. Four satellites insure complete coverage of the Earth surface.

It is expected that, in the absence of clutter, this radar could detect a rainfall rate of 2 mm/hr. Over water, this minimum value increases to a rate of 3.1 mm/hr; over land, to a rate of 8.0 mm/hr.

To improve the sensitivity in clutter conditions, Stepanenko proposes a dual-band radar much like that proposed by Keigler and Krawitz (ref. 4–21). Advantage is taken of the different variation with frequency of the strength of the clutter and the precipitation echoes. The dual-frequency radar is assumed to operate at wavelengths of 3 and 0.8 cm; identical antenna patterns are assumed. The peak power at 3 cm is 300 kW; at 0.8 cm, it is 30 kW. With these specifications, the minimum detectable rainfall rate over the sea is 0.7 mm/hr.

Stepanenko also considers the possible

characteristics of a radar in synchronous orbit. With a beamwidth of 0.43°, a peak power of 300 kW, a minimum detectable signal of 10^{-15} W, and a pulse duration of 1 μsec, a rainfall rate greater than 4 mm/hr can be detected with the radar wavelength being either 0.8 or 2 cm, but not 0.3 cm. The beam resolution in the tangential dimension is 80 to 90 km; in the radial direction, it varies from 0.2 to 6.5 km with the scan angle increasing from 0.2° to 7°. Stepanenko also states that, in future years, it should be possible to measure the rainfall intensity in addition to simple detection.

In the period since Dennis' study, dramatic advances in radar technology and significant developments in the atmospheric sciences have occurred. Among the latter are the development and use of numerical models for weather prediction and the modeling of cloud and precipitation processes from cloud scale to synoptic scale. Thus, it seems reasonable to reexamine the situation to determine whether meaningful satellite weather radar experiments or applications can be defined in terms of these more recent developments.

The fundamental limitation noted by Dennis is that the "snapshot" views of the precipitation distributions provided by weather radar on an orbiting satellite cannot be extrapolated very far in either space or time because of the inherent time and space variability of precipitation. Thus, Dennis believed that the utility of such observations for weather analysis and forecast purposes would be virtually insignificant. The precipitation observations differ greatly in this respect from the once- or twice-a-day observations of pressure, temperature, humidity, and windfields that are vital in weather forecasting, whether done by manual methods or with the aid of numerical models. There is considerable validity to Dennis' arguments; and, before embarking on a satellite radar project, it may be well to consult the meteorological community concerning the potential usefulness of global precipitation observations in the "snapshot" format.

Dennis suggested that at least 10 observations would be needed during the lifetime of meteorological systems to derive much meaningful information. With observations available on a once- or twice-a-day basis, this suggests that one should concentrate his attention on storms with lifetimes on the order of a week or more. This implies that the primary targets of interest will be persistent cyclonic storms, including hurricanes and typhoons and also extratropical cyclonic storms, many of which have durations sufficient to permit the acquisition of 10 or more sets of observations. An alternative would be to use a constellation of weather radar satellites to increase the frequency of observation.

Tropical storms are perhaps the easiest meteorological targets to observe from a satellite. Their size makes them easy to find, and their persistence makes it possible to acquire repetitive observations from low-altitude satellites. The fact that these storms spend most of their lifetimes over water simplifies the technological problems of separating rain-echo signals from surface-echo clutter. Satellite-borne weather radar observations on a once- or twice-a-day return cycle would provide a history of the development and distribution of precipitation within the storms during their entire lifetimes. Such observations are not available from other sensors or other weather radar platforms.

Satellite-borne weather radar observations of tropical storms, especially over the remote oceans, would aid research into the genesis and behavior of such storms and aid in attempts to develop physical and numerical models describing them. The observing capability could be used to support large-scale research programs such as GATE, FGGE, or Project Stormfury (concerned with hurricane modification by silver iodide seeding, which is scheduled to be resumed in the Pacific Ocean in 1976). Data from meteorological radars aboard orbiting satellites could provide valuable observations for such research efforts. The horizontal distribution of precipitation over the oceans can be obtained from microwave radiometric observa-

tions; thus, any satellite-borne weather radar system should probably be complemented by a radiometer on the same spacecraft, with possible use of the same antenna and maybe the same receiver front end for the two systems.

Some significant characteristics of tropical storm systems are outlined in table 4–II. Table 4–III gives estimates of the minimum and the desired radar observational capabilities to provide useful information for hurricane studies. The minimum requirements are based primarily on the characteristics of present-day numerical hurricane models. In general, these models are concerned only with two-dimensional distributions of precipitation or with a vertical structure represented by a small number of levels. Microwave radiometer techniques appear to be capable of meeting the minimum requirements for two-dimensional mapping of precipitation over water.

The desired observing capabilities are based on anticipated future development of hurricane models and extrapolation from the capabilities of presently available ground-based weather radar systems. Here, much finer resolution is specified in the horizontal direction, with still somewhat finer resolution generally being desirable in the vertical dimension. The necessary vertical resolution can only be achieved by use of active microwave techniques. Whereas nonattenuating wavelengths would be required to obtain quantitative echo-intensity measurements, the acceptable range of wavelengths for satellite-borne radars extends to much shorter values than is the case for ground-based weather radars. (See the section entitled "Attenuation Considerations.")

TABLE 4–III.—*Capabilities Needed for Satellite Radar Observations of Tropical Storms*

Minimum capability:	
Determine the two-dimensional (horizontal) distribution of precipitation echoes with resolution as follows:	
Horizontal, km	20
Time, hr	12
Reflectivity factor	semiquantitative
Desired capability:	
Determine the three-dimensional distribution of precipitation echoes with resolution as follows:	
Horizontal, km	2
Vertical, km	1
Reflectivity factor, dB	3
Time, hr	12
Determine wind velocities with resolution as follows:	
Horizontal, km	[a] 2
Vertical, km	1
Wind velocity:	
Magnitude, m/sec	2.5
Direction, deg	20
Determine storm movement with resolution as follows:	
Magnitude, m/sec	1
Direction, deg	10

[a] For some purposes, the horizontal resolution requirements of the wind measurements can be relaxed to 10 to 20 km.

The observing capability required for any specific investigation has to be determined by reference to the detailed scientific objectives. Thus, the present estimates indicate design goals that may serve as a basis for deciding whether the needed capabilities can even be approached by satellite-borne weather radar systems.

TABLE 4–II.—*Some Characteristics of Tropical Storm Systems*

Typical overall dimensions of precipitation region:	
Diameter, km	560
Height, km	18
Lifetime, weeks	1 to 3
Reflectivity factor range of interest, dBZ[a]	20 to 70
Windspeed, m/sec	0 to 75

[a] $dBZ = 10 \log_{10} Z$ (where Z is radar reflectivity factor in mm^6/m^3).

Concerning the modeling of hurricanes, the present numerical models (refs. 4–25 to 4–31) attempt to describe the development of the hurricane, and some of them include precipitation fields as part of the output. The models do not use precipitation data as input (ref. 4–32), but precipitation observations from a satellite weather radar would be one source of data against which to verify the models. Such observations might also be used to help periodically update the models as they simulate the life cycles of the storms.

The latent heat released during the formation of precipitation affects the air temperature, which, in turn, influences the storm dynamics. The height at which the heat is released is therefore very important in the numerical hurricane models. If it is released at low levels, a much stronger vortex circulation develops. To the extent that the latent heat release can be localized on the basis of radar observations of precipitation, satellite weather radar observations could provide additional important information for the verification (or revision, if necessary) of the models and perhaps also for use in updating models operating in real-time applications. The difficulty is that most of the latent heat is released during the condensation of water vapor to form cloud droplets. It may or may not be possible to relate observed regions of precipitation to the regions of latent heat release.

The development of hurricane numerical models has been fairly recent, and it can be reasonably expected that significant advances in the models will occur during the next decade. Previous experience has shown that it takes approximately 5 yr to advance a numerical model that involves precipitation processes to the point at which it is suitable for meaningful comparisons with actual observations of the hurricane models.

Many extratropical cyclonic storms also persist long enough to allow significant repetitive observations from orbiting satellites. However, the development of numerical models for such storms incorporating the precipitation process lags behind the work on tropical storms. Consequently, requirements for observing precipitation distributions in extratropical cyclones would apparently have to be based mainly on proposed uses in forecasting applications.

Applications of Satellite Weather Radar Observations

It is proposed that the meteorological information obtainable from a satellite-borne conventional pulse radar would include global mapping of rainfall intensity, measurements of storm maximum echo heights, and measurements of the height of the melting layer, which is characterized by a significant increase of radar signal intensity (bright band) observed mainly in stratiform precipitation. Rainfall intensities are now being mapped over the oceans by the ESMR installed on Nimbus 5. Thus, the principal value of an active microwave system would be to provide height resolution and thus allow the three-dimensional mapping of precipitation (i.e., inside cyclonic storms, as discussed in the section entitled "Weather Radar Observations From Orbiting Satellite Platforms"). In the absence of a vertical resolution capability, however, the active system provides little advantage over passive radiometric techniques. Over the oceans, radar could probably distinguish rain echoes from sea clutter to a distance of approximately 200 km from the subsatellite point. This distance is reduced to less than 800 km for precipitation over land.

In the future, satellite weather radar observations may be valuable in providing precipitation distributions for use as input to the numerical weather prediction (NWP) models. The horizontal grid spacing of the present NWP models is basically incompatible with the spatial variations of precipitation as observed by radar, the former being much too large. Partly because of this, the NWP models do not presently use precipitation data as input. In fact, moist convection and precipitation processes are just being incorporated into such models as the

limited fine mesh (LFM) model of the National Weather Service.

However, the precipitation process contributes a significant amount of latent heat in the atmosphere. This heat can be insignificant over the short term of a few days, but it could become increasingly important for longer periods.

Latent heat is not now an input for numerical weather prediction. Many numerical modelers consider the effects of precipitation to be second order in the models; thus, bringing the effects into the models would probably not have a major impact on the prognoses; however, there are suggestions to the contrary (ref. 4–33). Tracton's work suggests that an ability to identify local areas of strong convection and their relationship to regions of cyclogenesis would be helpful in improving the numerical forecasts. If that is the case, the models will eventually advance to the stage at which they can accept precipitation data as input. In that event, the global coverage obtainable from an orbiting satellite would be a definite asset. Modification of the numerical models and testing with available global rainfall data would be required before global rainfall data on an operational basis could be properly utilized.

The maximum echo height is a good indicator of the intensity of a storm. Rain associated with middle-latitude cyclonic storms has maximum echo heights ranging from 5 to 8 km. Thunderstorms have maximum heights generally above 10 km; hailstorms, above 13 km. Severe storms with tornadoes may exceed 20 km. Comparisons of the distribution of maximum echo heights in both tropical and extratropical storms at 12-hr intervals may indicate storm development or dissipation during the period. The maximum echo height is also a good indicator of the rate of rain production in convective storms.

The height of the melting layer is detected by radar as a "bright band," which is characterized by a significant increase of radar reflectivity at this level due to the partial melting of frozen hydrometeors. The 273-K level is generally located approximately 300 m above the peak of the bright band. A downward-looking radar can be expected to measure the height of the 273-K level to an accuracy of 200 m (to approximately 50 km from nadir). The accuracy will decrease to approximately 1 km at 150 km and to 2 km at 300 km. Further analysis of accuracy at different distances for nadir is required.

The heights of the 273-K level in rain should be useful as an input in numerical weather prediction. Temperature soundings of the atmosphere are now being determined from infrared and passive microwave measurements in satellites. However, these soundings can only be made in clear or partly cloudy regions. The heights of the 273-K level in rain areas would provide useful supplementary information.

The height of the melting layer would also be useful as a measure of the intensity and state of development of tropical storms and some extratropical storms. Tropical storms are initially "cold core," and they develop into hurricanes as "warm core." The resulting horizontal temperature gradient is a measure of the intensity of the storm. Measurements of the height of the melting level in different parts of the storm can be used to determine the temperature gradient.

Another possible application of weather radar observations from an orbiting satellite is in developing a global climatology of precipitation echoes. This application uses the synoptic observing capability of the satellite-borne radar system and, by concentrating on climatology, circumvents its limitation to "snapshot" observations. Radar climatological information is useful in a variety of military, communication system design, and other applications. To develop the necessary climatology, the satellite radar observations would have to be made in conjunction with visible and infrared observations of the same weather systems, preferably from geostationary satellites. Moreover, for many regions of the world, weather radar observations providing a sufficient basis for developing the climatology may already exist.

Satellite Radar for Meteorological Observations

There are three possible methods for configuring a radar in a low- or medium-orbit satellite for meteorological observations:

1. A fixed side-looking fan-beam antenna that provides the greatest swath width and has the simplest antenna system. However, this system requires larger power than other systems because of the wide swath. The wide elevation beam means that it cannot obtain height information about the precipitation, nor can it obtain a measure of the precipitation intensity because the degree of beam filling is unknown. Two antennas looking out opposite sides of the spacecraft can increase the coverage. This system operates over water better than over land because the background clutter is less over water.

2. An antenna beam that rotates continuously and provides at least two looks at the target (once when the satellite is approaching and once when it is receding). Either a fan-beam antenna or several contiguous pencil beams can be used to achieve the desired coverage. Generally, the coverage of a rotating antenna is slightly less than that of a fixed side-looking antenna. A possible variation of this type of system is one that scans a sector forward or aft of the satellite.

3. A downward-looking scanning pencil-beam antenna that covers a swath usually less than that obtained with the previous two solutions and requires a more complicated antenna. This system has the advantage of allowing measurement of the precipitation height and, because the precipitation usually fills the resolution cell, measurement of the precipitation intensity.

Each approach to satellite meteorological radar design has its particular advantages and limitations. The downward-looking scanning pencil-beam system is selected here as offering the most appropriate solution for meteorological observations. This system has the advantage of being able to map the distribution of precipitation in three dimensions.

The characteristics of a downward-looking scanning pencil-beam radar are listed in table 4–IV. Rather than describe the logical development of the radar design, brief comments will be offered to explain why these parameters were chosen. The major design criteria that had to be observed are (1) there should be sufficient signal-to-noise ratio (SNR) available for detecting a reasonable amount of precipitation, (2) the radar resolution cell (beamwidth and pulse duration) must be sufficiently small to exclude ground echo, and (3) the radar must be able to provide vertical resolution of approximately 1.5 km.

The radar operations frequency of 35 GHz was chosen to take advantage of the smaller antenna and the larger radar reflectivities possible at the higher frequencies. Satisfactory operation can also be achieved at a lower frequency. The reflectivity of precipitation does not increase as rapidly with increasing frequency above 35 GHz, and suitable components are more difficult to achieve.

To obtain good height resolution, the beamwidth must be small. A 0.2° beamwidth was selected as being the smallest that is likely to be achieved in the near future with a spaceborne antenna at that wavelength. This corresponds to an antenna that is 300

TABLE 4–IV.—*Characteristics of a Satellite Meteorological Radar Using a Downward-Looking Scanning Pencil-Beam Antenna*

Frequency (0.86-cm wavelength), GHz	35
Antenna beamwidth (conical beam), deg	0.2
Antenna size (diameter), m	2.6
Transmitter power:	
Average, W	16
Peak, kW	3.5
Pulse duration, μsec	2
Pulse repetition frequency, Hz	2300
System noise temperature, K	3000
System losses, dB	6
Scanning angle (from nadir), deg	45
Minimum rain intensity (with 13-dB SNR), mm/hr	2 (or 28 dBZ)
Swath coverage (from nadir), km	400
Orbit height, km	400

wavelengths in diameter. The pulse duration has a lesser effect on altitude resolution than the beamwidth; a value of 2 μsec was selected. With this beamwidth and pulse duration, the altitude resolution at nadir (along the groundtrack) is 0.6 km and increases to 1.5 km at 400 km for the groundtrack at the edge of swath coverage.

The orbit height of 400 km was chosen somewhat arbitrarily and should be examined further to determine optimum orbit coverage. The 400-km orbit height and the need for 1.5-km height resolution results in a swath of 800 km (400 km on either side of the groundtrack). This is the approximate coverage needed with one satellite to insure one observation per 12 hr. To obtain a revisit time of 3 hr, four such satellites are required.

One of the most unusual aspects of this radar design is the high PRF. An ambiguous range is accepted in this design to obtain continuous ground coverage. If there is to be one pulse per beam position and if the satellite is to travel no more than one resolution cell in the scan time, the PRF must be 2300 Hz. This PRF corresponds to an unambiguous range of 65 km. Atmospheric precipitation will extend over a range interval smaller than 65 km; thus, there is no "foldover" of the rain echo and no ambiguity as to the determination of the true range. To achieve quantitative measurements of precipitation echo intensity with a single pulse-per-beam position, some form of coding will be needed on the transmitted waveform.

However, one important antenna design factor must be considered as a consequence of such a high PRF. When the radar echo returns to the satellite, the transmitting beam is looking at some other part of its coverage. Thus, there must be separate receiving and transmitting beams displaced in angle. With an orbiting satellite at an altitude of 400 km, the separation is approximately 3.3 beamwidths at the nadir and 4.7 beamwidths at the edge of the swath coverage. This factor complicates the antenna design, but it should be possible to achieve.

The minimum detectable rain intensity with this system is 2 mm/hr, corresponding to a reflectivity factor Z of 28 dBZ.[1] This could be traded with transmitter power. If the minimum detectable rain is increased to 4 mm/hr, then the average power can be reduced to approximately 5 W.

The most demanding component of the radar is the antenna. The type of antenna needed might be obtained with a frequency-scan linear array feeding a parabolic cylinder, an organ-pipe scan feeding a parabolic torus or a two-dimensional lens, or a mechanically rotating set of four switched paraboloid reflectors. The frequency-scan linear array feed is attractive because of its simplicity. The displacement of transmit and receive beams might be achieved by simply tuning the receiver to a different frequency than the transmitter. The possible limitations of the frequency-scan antenna are the wide bandwidth needed for the 2-μsec pulse and the possible high loss in the transmission line (snake feed).

This design of meteorological radar also has utility for Earth-sensing applications other than the atmosphere; that is, it can be used as a scatterometer or even as a precision altimeter with the inclusion of pulse compression.

Attenuation Considerations

Microwave attenuation is relatively small for a satellite-borne radar compared to that for ground-based radar. In the case of widespread precipitation, the reflectivity factor Z in rain is constant below the melting layer, and it is sufficient to measure Z in the upper portion of the rain to determine rain intensity. In the melting layer, attenuation may be increased perhaps by a factor of 3 over that of rain, but the depth of this layer is only approximately 400 m; thus, the total attenuation is relatively small. Above the 273-K level, the attenuation for snow is one-tenth or less that of rain and can generally be neglected.

In thunderstorms, supercooled water can exist at very low temperatures. However, the

[1] $\mathrm{dBZ} = 10 \log_{10} Z$.

probability of freezing increases with drop size and decreasing temperature. A 1-mm-diameter raindrop has a high probability of freezing at 263 K; a 0.5-mm-diameter raindrop, at 259 K. The greatest attenuation would be expected in a hailstorm in which wet hail can exist at temperatures as low as 258 K. However, the portion of a thunderstorm containing large raindrops or wet hail at temperatures below 263 K is limited to small horizontal regions ($\approx$5 km). In addition, the reflectivity factor, at an altitude of approximately 6 km (temperature approximately 258 K) in severe storms containing supercooled water or wet hail, exceeds 50 dBZ and is approximately the same as that in rain below the 273-K level. Therefore, a measurement of a Z value exceeding 50 dBZ at 6 km is indicative of a severe storm. The attenuation above the 6-km level generally will be relatively small.

In summary, attenuation will not normally be a problem in measuring precipitation reflectivity from a satellite above 6 km (in the case of convective storms) and below the 6-km level (in stratiform), even at wavelengths as low as 8 mm. In limited areas associated with severe storms, there may be moderate attenuation so that the value of the reflectivity at 6 km may be underestimated. More information on attenuation characteristics in the upper portions of severe storms is desirable.

Use of a Geostationary Satellite as a Weather Radar Platform

A satellite-borne weather radar system can be used to study, for the first time, the evolution and migration of precipitation in large-scale tropical storms. However, for truly effective monitoring of precipitation, it is necessary to scan a large area rapidly, perhaps once every 15 min when a storm is developing.

The requirements of large-area coverage and frequent observations dictate the use of a geostationary satellite for the radar system platform. Unfortunately, the orbit height (36 000 km) of such satellites places severe constraints on the performance parameters for a useful system.

A radar system designed for monitoring severe weather conditions should be capable of a horizontal resolution of approximately 10 to 20 km and a vertical resolution of 1.5 km. The total power consumption of the system should be low, and the size and weight of the antenna should be minimized. These considerations dictate the use of a short-wavelength (3 to 9 mm) radar system or even a CO_2 laser system such as the one discussed in the section entitled "Carbon Dioxide Pulsed Continuous-Wave Doppler Radar." However, optical radiation does not penetrate clouds.

Of course, even the millimeter wavelengths are strongly attenuated by atmospheric water vapor and oxygen (see the section entitled "Atmospheric Transmission and Ocean Reflectivity in the Neighborhood of the 5-mm Oxygen Band"), so the operating wavelengths should be carefully selected to be in an atmospheric window. At millimeter wavelengths, the state of the art of microwave device development is not as advanced as at the longer centimeter wavelengths; consequently, some components are not generally as reliable or readily available. However, received sensitivity is approximately the same at 3 mm as at 9 mm, and it is believed that there are no severe technological limitations in using short-wavelength radar.

In fact, existing systems have adequate performance characteristics to permit storm detectability from geosynchronous altitudes. For example, a 3-mm radar system using a 4-mm-diameter antenna could easily detect a tropical storm and measure maximum echo heights on a more or less continuous basis. Such a radar operating at an altitude of 36 000 km would be capable of 1-km vertical resolution at the nadir, which would be adequate for meteorological purposes. However, to achieve a reasonable horizontal resolution of 30 to 40 km requires a beamwidth of approximately 1 mrad, which is beyond the reach of technology in the near future.

The major obstacle in using a geostationary

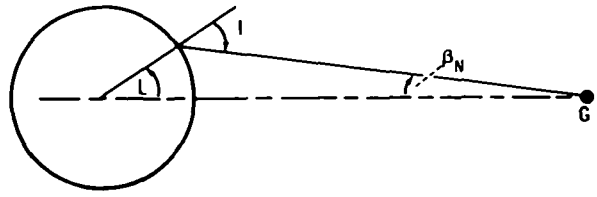

FIGURE 4–3.—Geometry of a geostationary platform, where I is inclination, β_N is nadir angle, and L is latitude.

platform is the problem faced by all side-looking ranging systems (namely, the loss of height resolution when scanning away from the nadir). The geometry of the situation is illustrated in figure 4–3; the relationship between latitude and the apparent inclination of the radar beam from the vertical is shown in table 4–V.

Even with a large 9-m parabolic antenna, which would possibly have an angular resolution of 0.5 mrad, the echo-height ambiguity is greater than +1.5 km for storms at a latitude of only 11°, simply because of geometric effects. Larger uncertainties would obviate the use of the system for measurements of maximum echo height.

It appears that angular resolutions of approximately 0.1 mrad, which could be achieved with the CO_2 lidar discussed in the section entitled "Carbon Dioxide Pulsed Continuous-Wave Doppler Radar," would be required to obtain useful meteorological information at a latitude of 45°. Until the deployment of large linear antenna arrays becomes a practical possibility, the angular resolution problem inherent with microwave systems may essentially limit the use of geostationary platforms to the study of equatorial weather.

TABLE 4–V.—*Variation of Inclination With Latitude*

Latitude, deg	Nadir angle, deg	Inclination from vertical, deg
5.6	1	6.6
11.4	2	13.4
17.3	3	20.3
23.6	4	27.6
30.4	5	35.4
38.0	6	44.0
47.0	7	54.0
59.5	8	67.5

MULTIWAVELENGTH AND DUAL POLARIZATION RADAR FOR WEATHER DETECTION FROM SATELLITES

This section concerns possible improvements of radar capabilities for the observation and measurement of precipitation by the use of two or more operating frequencies. The concept of multifrequency radar has been discussed in the literature (refs. 4–34 to 4–36) and is introduced in this section with the expectation that it will become feasible in a time frame of 5 to 10 yr and may contribute to a more accurate determination of precipitation and clouds.

At present, radars are used to detect precipitation and, in fact, to determine rainfall intensity. These determinations are made by assuming a relationship between rainfall rate and radar reflectivity, which is determined empirically. Unfortunately, there is no unique relationship between these two parameters because they vary with the raindrop distribution in different ways. Different droplet distributions can result in the same rainfall rate and still yield different radar reflectivities. It is therefore necessary to find additional parameters measured simultaneously that will resolve the uncertainty.

A parameter that is being proposed is radar-signal attenuation. It will be shown that, if reflectivity is estimated at both attenuating and nonattenuating wavelengths, rainfall rates can be determined with greater accuracy.

Another parameter is polarization. Larger raindrops are more oblate in shape than smaller raindrops, which are more nearly spherical. It is known that nonspherical raindrops cause depolarization of electromagnetic waves. Thus, although quantitative analysis has yet to be made, it is likely that polarization measurement will improve the knowledge of drop size.

Although all other techniques in this section apply to low-altitude satellites, it is also suggested that information on drop-size spectra can be obtained using a Doppler radar from a geostationary satellite.

Because cirrus clouds result in very small attenuation values but are detectable with ultrasensitive radars, their presence can also be determined by simultaneous measurements of reflectivity and attenuation at different frequencies.

Backscatter, Attenuation, Drop-Size Spectra, and Error Analysis

The weather radar equation can be expressed in the following form (ref. 4–11):

$$P_r=\frac{C_1}{R^2}\sum_i \sigma_i \tag{4–1}$$

where P_r is the power received from a volume of atmosphere containing precipitation, C_1 is a constant containing the fixed radar parameters, R is the radar range, and σ_i is the radar cross section of the ith droplet. The value of σ for an individual water drop of diameter D is given by the Rayleigh expression for cross section

$$\sigma=\frac{\pi^5}{\lambda^4}|k|^2D^6 \tag{4–2}$$

where $d\ll\lambda$, λ is the radar wavelength, and the atmospheric attention coefficient k is

$$k=\frac{m^2-1}{m^2+2} \tag{4–3}$$

where m is the complex index of refraction.

Equation (4–2) is valid for rain if λ is greater than approximately 5 cm. For smaller λ, the more complex Mie theory must be used to obtain the correct radar cross section, which is given by

$$\sigma=\frac{\pi D^2}{4\alpha^2}\left|\sum_{i=1}^{\infty}(-1)^i(2i+1)\,(a_i-b_i)\right|^2 \tag{4–4}$$

where the rain attenuation coefficient α is $\pi D/\lambda$, and a_i and b_i are coefficients that depend on the refractive index and α.

Equation (4–1) can also be written

$$P_r=\frac{C_2|k|^2}{R^2}Z \tag{4–5}$$

where

$$Z=\sum_i N_iD_i^6 \tag{4–6}$$

where Z is the reflectivity factor (conventionally expressed in mm^6/m^3, N_i is the drop-size distribution (m^{-3}), and D is the raindrop diameter (mm). For non-Rayleigh scattering, the effective radar reflectivity factor Z_e should be substituted for Z. The reflectivity η is the backscattering cross section per unit volume and is given by

$$\eta=\frac{\pi^5}{\lambda^4}|k|^2Z_e \tag{4–7}$$

The liquid-water content M_w is given by

$$M_w=\rho_w\frac{\pi}{6}\sum_i N_iD_i^3 \tag{4–8}$$

where ρ_w is water density.

If the radar wavelength is less than approximately 5 cm, the attenuation must be taken into account when clouds and rain exist over the transmission path. Gunn and East (ref. 4–37) give the following expressions for the attenuation due to Mie scattering cross section Q_s, absorption cross section Q_a, and total droplet cross section Q_t for rain and clouds.

$$Q_s=\frac{\lambda^2}{2\pi}\sum_{i=1}^{\infty}(2i+1)\,(|a_i|^2+|b_i|^2) \tag{4–9}$$

$$Q_t=\frac{\lambda^2}{2\pi}(-\mathcal{R}\varepsilon)\sum_{i=1}^{\infty}(2i+1)\,(a_i+b_i) \tag{4–10}$$

and

$$Q_a=Q_t-Q_s \tag{4–11}$$

Calculations of Q_t have been made by Haddock (ref. 4–38) and Medhurst (ref. 4–39), from which estimates of total attenuation can be made. The total attenuation will depend on the number density of raindrops and is represented by

$$\kappa=\int_0^{\infty}Q_t(mD)n(D)\,dD \tag{4–12}$$

where κ is attenuation in dB km^{-1}, Q_t is in units of dB km^{-1} cm^3, and $n(D)$ is the number

of drops per cubic centimeter in the size range dD.

Measurements of attenuation by different investigators show moderately good agreement at various wavelengths between 0.6 and 10 cm (ref. 4–40). In terms of available data, one may conclude that the theory is completely adequate. It is quite likely, however, that the spread in the experimental measurements is explained by the spatial variations in precipitation and drop-size distributions.

Drop-size distributions generally follow the Marshall-Palmer (ref. 4–41) distribution, which is expressed by

$$n(D) = n_0 \exp(-\Lambda D) \qquad (4\text{–}13)$$

where n_0 and Λ are constants. It should be clear from equations (4–6) and (4–12) that, if the exact drop-size distribution is known and the radar beam is filled, the values of radar reflectivity and attenuation are uniquely established. This suggests the possibility that if Z and the attenuation coefficient k are measured at two or more electromagnetic wavelengths, then the drop-size distributions can be determined. This concept is developed by Goldhirsh and Katz (ref. 4–36), in which two radars at different frequencies are used to measure Z and k simultaneously to obtain drop distributions in rain. The analysis of this concept is as follows.

Two simultaneous equations are derived, one representing reflectivity at a nonattenuating wavelength (i.e., S-band) and the other representing attenuation at a shorter (attenuating) wavelength (i.e., X- or K-band). Let P_{10} and P_3 be the powers received from the same precipitation at S-band (10 cm) and X-band (3 cm), respectively. One can then determine that

$$P_{10}(R) = \frac{C_{10} Z(R)}{R^2} \qquad (4\text{–}14)$$

and

$$P_3(R) = \left[\frac{C_3 \eta_3(R)}{R^2}\right] 10 \exp\left(-0.2 \int_0^R k_3 \, dR\right) \qquad (4\text{–}15)$$

where η is normalized reflectivity, the subscripts 10 and 3 refer to radar wavelengths in centimeters, and C is the radar constant for each radar.

Consider now a range interval ΔR equal to, or greater than, the pulse length. If the reflectivity is uniform over ΔR, one can determine the attenuation in terms of the backscattered power.

$$k_3 = \left(\frac{5}{\Delta R}\right) \log\left[\frac{R^2 P_3(R)}{(R+\Delta R)^2 P_3(R+\Delta R)}\right] \qquad (4\text{–}16)$$

One can also find k_3 by substituting equation (4–13) into equation (4–12):

$$k_3 = n_0 \int_0^\infty Q_{t_3}(D) \exp(-\Lambda D) \, dD \qquad (4\text{–}17)$$

in which the unknowns are n_0 and Λ, and $Q_{t_3}(D)$ is total attenuation at 3 cm.

Using the fact that, at S-band, Z depends on the sixth power of D, one can determine that

$$Z_{10} = n_0 \int_0^\infty D^6 \exp(-\Lambda D) \, dD = \frac{N_0 6!}{\Lambda^7} \qquad (4\text{–}18)$$

Note that equation (4–18) is also only a function of n_0 and Λ.

Dividing equation (4–17) by equation (4–18) gives

$$\frac{k_3}{Z_{10}} = \frac{\Lambda^7}{6!} \int_0^\infty Q_{t_3}(D) \exp(-\Lambda D) \, dD \qquad (4\text{–}19)$$

in which the left side is obtained by measurements at the two radar frequencies and the right side is a function only of Λ. Because $Q_{t_3}(D)$ is a known function of m (which depends on wavelength and temperature) and D, the right side is calculable. With Λ determined, n_0 is determined by using equation (4–17) or (4–18). These calculations show that the drop-size distributions can be determined; therefore, the precipitation characteristics in terms of rainfall intensity, radar reflectivity, and also liquid water can be effectively measured. It was only assumed that the radar beam is filled with precipita-

tion particles. The analysis leading to equation (4–19) can be repeated using any other attenuating wavelength.

The determination of Z at S-band requires a knowledge of the radar parameters (e.g., antenna and receiver gain, line losses, etc.) that comprise the radar constant C_{10} in equation (4–14). On the other hand, the determination of the attenuation coefficient k, as given by the form of equation (4–16), requires only a relative power measurement, and it therefore does not require a knowledge of these radar parameters. The measured ratio k/Z may contain errors primarily due to uncertainties in the S-band parameters. A method, which is described here, using two radars operating at attenuating wavelengths (K- and X-bands) as well as an S-band radar for surveillance can overcome this disadvantage. The general idea is to measure the attenuating coefficients over a common zone of uniform rain at both K- and X-bands. Through a comparison of these two independent measurements, the parameters n_0 and Λ may be ascertained as before.

Because the attenuating coefficients have the form of equation (4–17), the ratio k_1/k_3 is given by

$$\frac{k_1}{k_3}=\frac{\int_0^\infty Q_{t_1}(D)\exp(-\Lambda D)\,dD}{\int_0^\infty Q_{t_3}(D)\exp(-\Lambda D)\,dD} \tag{4–20}$$

in which the only unknown on the right side is Λ. The left side is obtained by a measurement of the powers of the two frequencies.

$$\frac{k_1}{k_3}=\frac{\log\left[\dfrac{R^2P_1(R)}{(R+\Delta R)^2P_1(R+\Delta R)}\right]}{\log\left[\dfrac{R^2P_3(R)}{(R+\Delta R)^2P_3(R+\Delta R)}\right]} \tag{4–21}$$

Again, after Λ is determined, n_0 is determined from equation (4–17).

In their initial treatment, Goldhirsh and Katz (ref. 4–36) performed an error analysis to determine the radar accuracy requirements. They estimated the error in Λ for ± 1-dB measurement errors and the rain-rate errors as given by the Marshall-Palmer distribution, assuming $n_0=0.08$. This procedure led to unacceptably large errors in rainfall rate. A more realistic analysis is described in which error bounds were obtained by allowing both Λ and n_0 to vary for selected radar measurement errors. From equations (4–17) and (4–18), one obtains one value for Λ and n_0 for a given set of values of Z and k_3. Taking Z to be in error by ± 2 dB and k_1 and/or k_3 to be in error by 25 percent or ± 1 dB (these are likely to be achievable in practice) allows the calculation of errors first in Λ and n_0, from which one can find rainfall-rate errors. These are shown in figure 4–4, where rainfall-rate error is plotted against actual rain rate for the various pairs of measurements (k_3 and Z, k_1 and Z, and k_1 and k_3). Notice that error bounds, using the k_1 and Z (at 10 cm) and the k_1 and k_3 combinations, are within reasonable limits. The k_3 and Z curves are clearly too large. The upper curve labeled "zero error in k_3" contains only the ± 2-dB error in Z. Clearly, as the radar accuracies are improved, so are the precipitation parameters. As stated later, the goals should be to achieve relative radar accuracies of approximately ± 0.2 dB, which

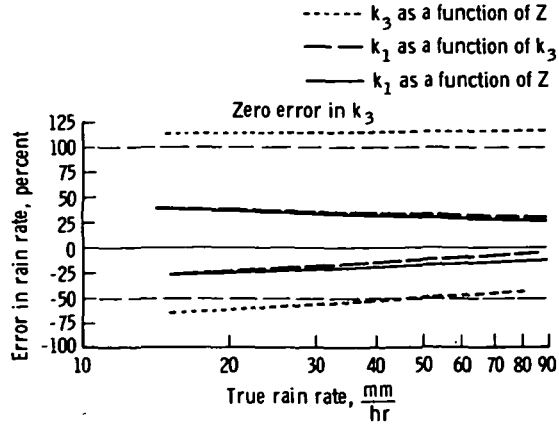

FIGURE 4–4.—Error in rain rate plotted against true rain rate for three pairs of measurements with a ± 2-dB error in Z and a ± 25-percent error in k (except the top curve, which contains only the ± 2-dB error in Z).

yield quite acceptable accuracies in drop sizes, liquid-water contents, and rain rates.

Determination of Optimum Wavelengths

The preceding discussion indicates that the attenuating wavelength should be as short as possible so that large attenuations per unit length (needed to obtain high accuracy from these multiple wavelength measurement methods) are obtained. It must be noted that, if the wavelength is too short, maximum penetration into the rain becomes a problem.

Two factors determine penetration. As the wavelength becomes shorter, the cross section of the rain increases as $1/\lambda^4$ in the Rayleigh region and somewhat slower in the Mie region. At the same time, the attenuation caused by the return from the rain at the maximum range of interest is increasing as $1/\lambda$. These two opposing factors cause the radar return to first rise with decreasing wavelength, go through a maximum, and then decrease. As the required penetration distance decreases, the wavelength at which maximum return is observed will shift toward shorter wavelengths. This is due to the decreasing influence of the attenuation factor as range decreases.

For a satellite-borne meteorological radar, the optimum wavelength will be much shorter than for a ground radar. Rain rarely extends above 10 km, except for large thunderheads and severe storm regions. Characteristic path lengths through rain will then be on the order of 10 km (or slightly more) to allow for normal incidence resulting from scanning.

In addition, the intensity of precipitation usually decreases with increasing altitude above the 273-K level. This relationship puts the least attenuating portion of the rain path closest to the radar and the most reflecting portion of the path farthest from the radar. This fact further enhances the ability to use short wavelengths.

In contrast to this situation, a ground radar should have a working range an order of magnitude greater than 10 km to measure rain over a satisfactory area. Furthermore, it is desirable to observe less dense rain beyond rain cores. As a result, radars at X-band, C-band, and even S-band are favored.

To determine optimum attenuating and nonattenuating wavelengths for the satellite case, the variation in the relative radar return from a resolvable element of rain seen through a uniform column of rain of length r is calculated by graphic means. The range of possible operating wavelengths is then determined by selecting the wavelength interval around the wavelength of maximum return that is not too far down from maximum to yield a good SNR.

The calculation can be done for a 10-km rain path length and for two rainfall rates (8 and 0.8 mm/hr). The range of operating wavelengths will be taken as those that are less than 16 dB down from the peak return at the greatest rainfall rate.

To calculate radar return against wavelength, observe that the return radar power P_r is given by

$$P_r = \frac{P_t G_t A_r V}{(4\pi R^2)^2}(\eta 10^{-2\alpha r})$$

$$= \frac{\frac{P_t 4\pi}{\Delta\phi^2} A_r (\Delta r R^2 \Delta\phi^2)}{(4\pi R^2)^2}(\eta 10^{-2\alpha r})$$

$$= \frac{P_t A_r \Delta r}{4\pi R^2}(\eta 10^{-2\alpha r}) \qquad (4\text{–}22)$$

where

P_t = transmitter power
G_t = radar antenna gain
Δr = range resolution
A_r = radar antenna cross section
R = radar range
r = range through rain
$\Delta\phi$ = antenna beamwidth
α = rain attenuation coefficient
V = volume of resolvable element of rain
η = rain reflectivity
λ = operating wavelength

The condition $A_r = 2\pi\lambda$ makes the beamwidth equal at all wavelengths. Then, the same resolvable element of rain will be observed at all wavelengths.

The input data are the values of η and α as a function of λ as given by Mitchell (ref. 4–42). These data, plotted with λ as a parameter and rainfall rate as the independent variable, were replotted with λ as the variable (for rainfall rates of 8 and 0.8 mm/hr). The resulting graphs of $\lambda^2\eta e^{-2\alpha r}$ for these two rainfall rates are given in figure 4–5 with $r=10$ km.

The optimum wavelength calculated by using the previously described method varies from approximately 1.8 cm (for 8 mm/hr) to 0.8 cm (for 0.8 mm/hr). If the attenuating wavelength return is allowed to fall no more than 10 dB below the peak return for 8-mm/hr rainfall, then the attenuating wavelength can be as short as 0.8 cm for the 8-mm/hr case. The wavelength shortens to approximately 0.5 cm for the 0.8-mm/hr case.

The nonattenuating wavelength for 8-mm/hr rainfall is approximately 5 to 6 cm (C-band) for which the response is less than 10 dB down from the peak response. However, for 0.8-mm/hr rainfall, the nonattenuating wavelength must be shorter. For $\lambda=3$ cm, the response is down 18 dB from the peak response of 40 dB for 8-mm/hr rainfall and $\lambda=1.8$ cm.

As noted before, the attenuating wavelengths are in the Mie region. This fact has an important consequence. If the nonattenuating and attenuating wavelengths were both in the Rayleigh region, measurement at two wavelengths would produce all the data obtainable. The Z value and attenuation at any other Rayleigh wavelength would be predictable from the measurements at the first two wavelengths.

However, if the attenuating wavelengths fall in the Mie region, it will become apparent from the following discussion that measurements done at other wavelengths permit the determination of additional parameters specifying drop-size distribution.

To determine whether the scatter is in the Mie region at 1-cm and 8-mm/hr rainfall, refer to the rain parameter diagram (ref. 4–43) in figure 4–6. Here, D_0 is the median

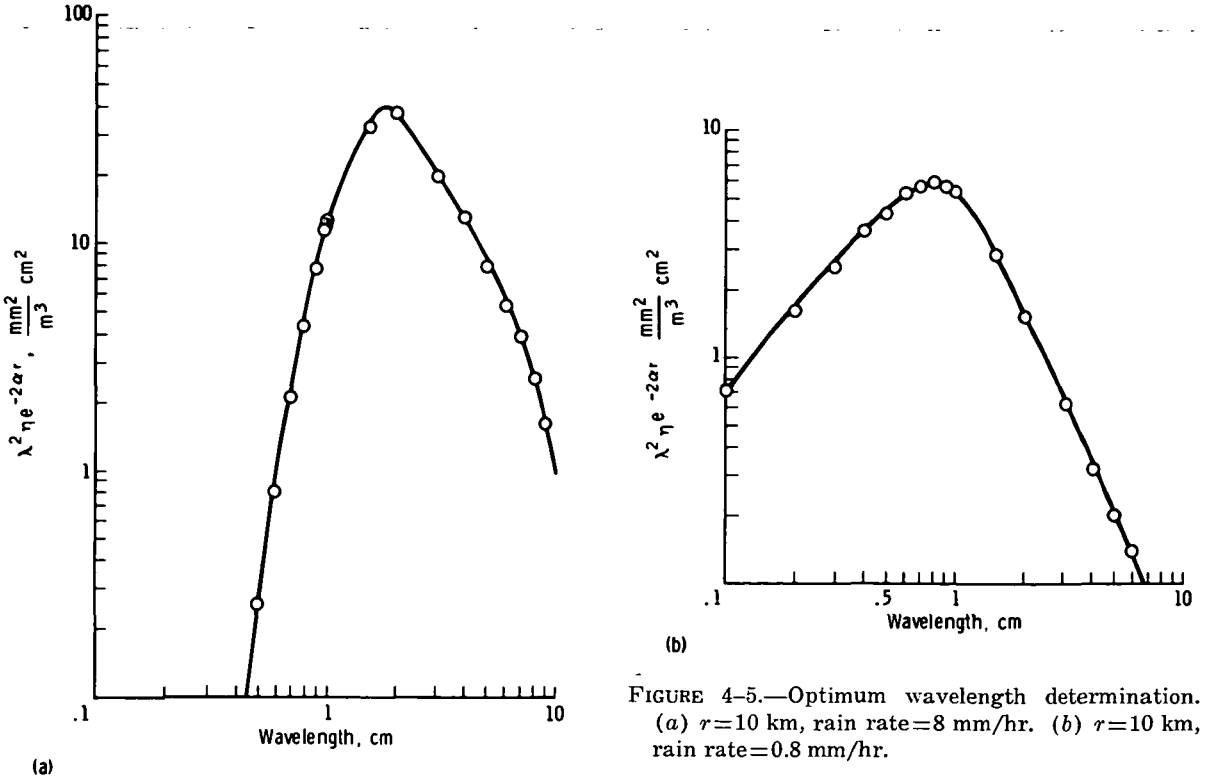

FIGURE 4–5.—Optimum wavelength determination. (*a*) $r=10$ km, rain rate=8 mm/hr. (*b*) $r=10$ km, rain rate=0.8 mm/hr.

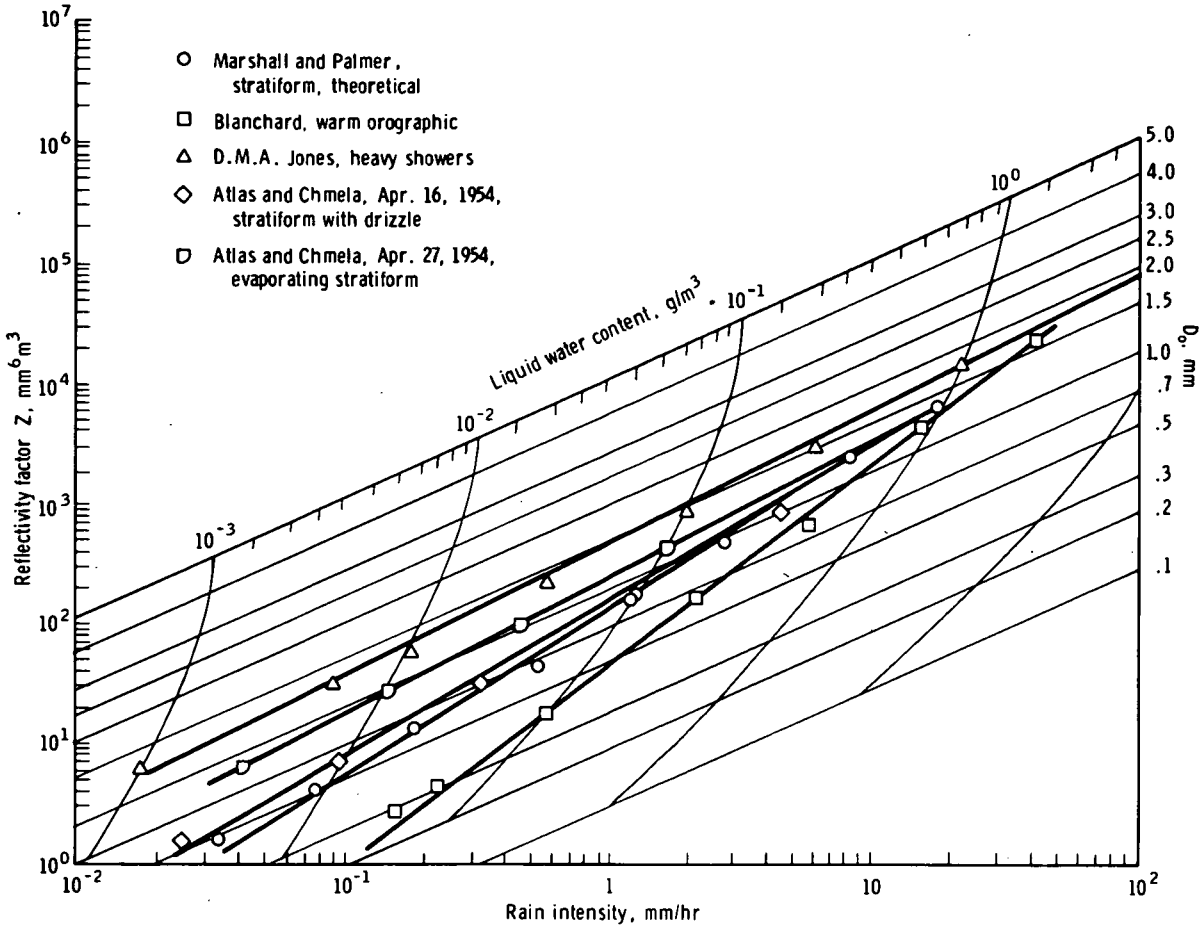

FIGURE 4–6.—Relationship of reflectivity factor Z, liquid water content, median diameter of the volume D_0 and rain intensity for a mean size spectrum (ref. 4–43).

diameter of the volume. For a rain intensity of 8 mm/hr, this diameter varies from 1.0 to 1.5 mm, depending on rain type.

Using an average value of $D_0=1.25$ mm, then $\alpha=\pi D/\lambda$ is 0.4 at $\lambda=1$ cm. Referring to a plot by Gunn and East (ref. 4–37) of the deviation of the attenuation and backscatter cross sections from Rayleigh (as a function of λ and α), it is seen that for $\alpha=0.4$ and $\lambda=1$ cm, the backscatter cross section is still very close to its Rayleigh value (fig. 4–7). However, the attenuation is about seven times greater than its Rayleigh value. This is a substantial deviation. Therefore, the scatter is in the Mie region for attenuation but not for target cross section. The attenuation constant is approximately 1.5 dB/km, giving a total attenuation increment of 3 dB for a 2-km path increment.

For 0.8-mm/hr rainfall, a shorter wavelength is required to get a substantial attenuation increment in 2 km. For this rate, the shortest practical attenuating wavelength is approximately 0.5 cm. Referring to the nomogram again, one sees that the median drop size is approximately 0.8 mm and α equals 0.58. Figure 4–7 shows that the attenuation differs from Rayleigh by a factor of 4.7. This is also a substantial deviation, as in the 8-mm/hr case.

If more operating wavelengths in the Mie region are available, simultaneous equations can be set up that take into account the deviation from Rayleigh of both cross section

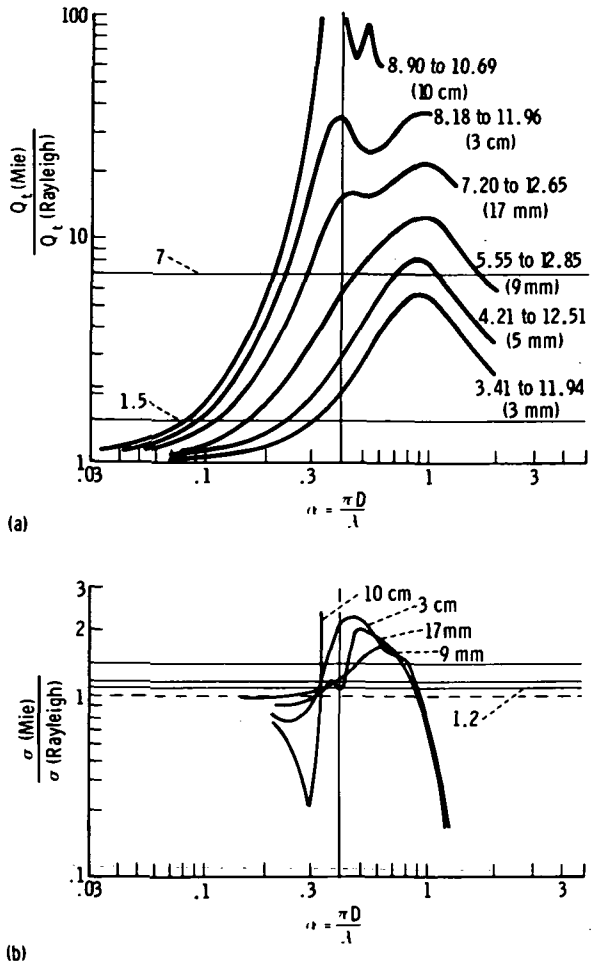

FIGURE 4–7.—Ratio of actual attenuation and actual backscattering to that given by the Rayleigh approximation for water at 291 K. (*a*) Ratio of actual attenuation to Rayleigh attenuation approximation. The complex refractive index and the wavelength (in parentheses) are shown for each curve. (*b*) Ratio of actual backscattering to Rayleigh backscattering approximation.

and attenuation. More parameters describing the deviation of the distribution from standard must be obtained to prevent overconstraint of the equation set. Indeed, the set of simultaneous equations is an approximation of an integral equation in which a finite number of data points are available. The standard distribution is then the preliminary estimate of the solution of the integral equation by recursion (successive approximations).

The number of radar frequencies used should obviously be at a minimum for a satellite application. However, the preceding discussion shows that wavelengths of approximately 0.5, 1, and 6 cm are needed to effectively measure rainfall intensities from 8 to 0.8 mm/hr. X-band and S-band may have to be added for very high rainfall rates (16-mm/hr and greater). Only a pair of these frequencies need to be operated simultaneously. The selection of a 0.5-cm wavelength must be avoided because it falls on the O_2 absorption band. However, a slightly different wavelength that still provides a satisfactory choice may be selected. Operation very close to an O_2 line in the absorption band may be advantageous. By selection of the correct wavelength, a situation may be obtained where the radiation is not greatly absorbed at high altitudes, but is heavily absorbed at low altitudes. This situation occurs because the O_2 line is narrow at high altitudes and therefore does not greatly attenuate the operating wavelength, which is offset from the line center as shown in figure 4–8.

At low altitudes, pressure broadening widens the O_2 band and attenuation becomes

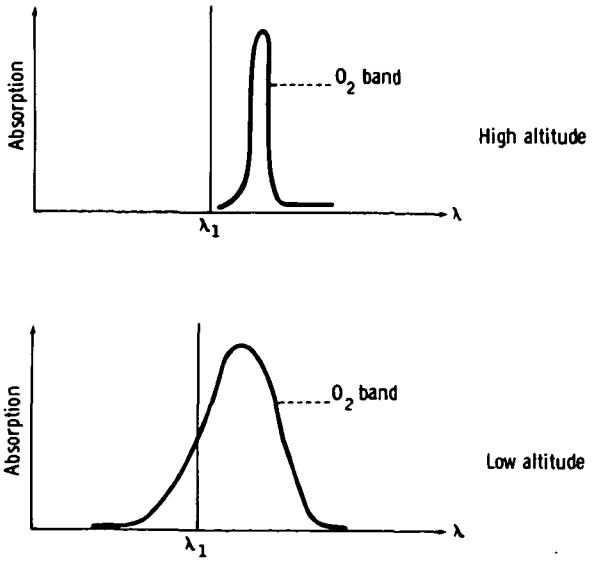

FIGURE 4–8.—Relationships of operating wavelength λ to the O_2 60-GHz absorption band.

very large. In the active microwave case, this may constitute a technique for eliminating ground clutter and thereby remove the swath-width limitation caused by the presence of ground clutter. In fact, by using a series of operating frequencies close to the center of an O_2 line, it may be possible to sound the atmosphere for precipitation without ranging, as in the passive case. This would be useful when large incident angles are used to obtain wide swath widths.

It should be mentioned that Atlas and Ulbrich (ref. 4–34) found that, in any case, the attenuating wavelength should be shorter than 1.5 cm so that the extinction coefficient will be independent of wavelength. This restriction may be a source of error when X-band must be used as the attenuating wavelength for extremely high rainfall rates.

Calibration

To increase the accuracy of the two-wavelength method for measurement of liquid-water content, it is desirable to calibrate the system. This calibration can be done by measuring the total attenuation through the rain path at selected calibration locations. Because the satellite radar has measured the total attenuation from maximum echo height to the Earth surface at the attenuating wavelengths, an independent measurement of the total attenuation will reveal any systematic errors in attenuation measurement that cause the two independent measurements to differ. The errors can then be removed or calibrated out, thereby improving the accuracy of the satellite system.

Primary calibration measurements would be made by measuring the intensity of the attenuating wavelength at ground stations. However, to get calibrations over a wider range of meteorological conditions, a second method is proposed that involves reflection of the satellite radar beam from the ocean surface.

The possibility of accurate determination of ocean-surface reflectivity depends on the unusual fact that the reflectivity of a smooth seawater surface is constant to a high degree of accuracy for angles of incidence up to approximately 40°. This condition occurs because circular polarization is composed of equal amounts of the linearly polarized components in the plane of incidence and normal to the plane of incidence. Brewster's angle for seawater occurs at an approximately 90° angle of incidence (i.e., 83° at 9 GHz and 283 K). The two linear polarizations deviate from their common reflectivity at vertical incidence, one increasing and the other decreasing. When Brewster's angle is near grazing, the rates of increase and decrease are approximately equal for a region around normal incidence. The average increase and decrease, observed by use of circular polarization, is almost constant in this region.

In figure 4–9, the emissivity E for smooth seawater is plotted for E_{par} (parallel), E_{per} (perpendicular), and E_{cir} (circular) polarization. The emissivity is almost constant to 40°. For a smooth surface, the reflectivity is 1 minus the emissivity; therefore, the plot indicates that the reflectivity for circular polarization is also almost constant to approximately 40°, which makes circular polarization applicable to radar measurements.

To apply this observation to the measurement of the molecular temperature of an

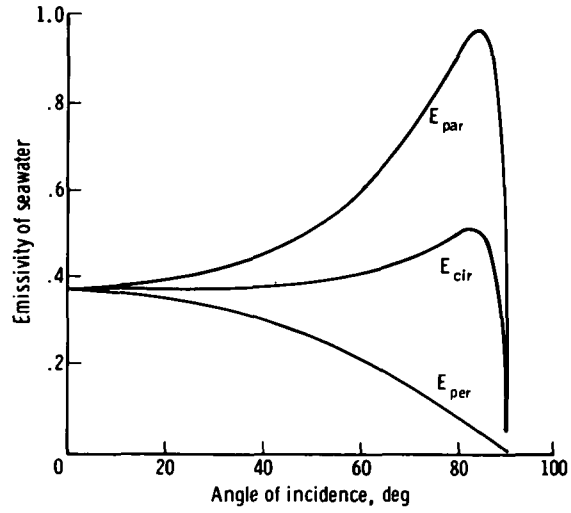

FIGURE 4–9.—Emissivity of smooth seawater plotted against angle of incidence for parallel, circular, and perpendicular polarizations.

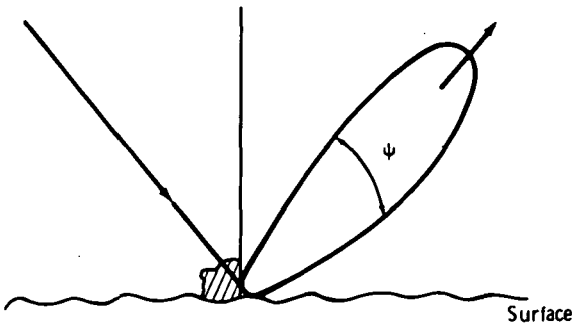

FIGURE 4–10.—Forward scattering by surface facets.

actual rough sea, the facet theory of reflection can be used. According to this theory, the incident beam will be scattered by the facets into a forward-scattered beam formed by specular reflection from the facets (Kirchhoff scattering) as shown in figure 4–10.

In addition, there is a pattern of diffracted radiation emanating in all other directions as shown by the crosshatching in figure 4–10. Obviously, the facet theory will be of little help in predicting the magnitude of the diffracted radiation. This diffuse radiation is scattered from irregularities having a size comparable to the radar wavelength (i.e., small ripples in the case of X-band).

In determining seawater temperature, it is assumed that all the power is in the forward-scattered lobe and that the power diffracted out of this lobe could be neglected. Because the sea-surface slopes do not exceed approximately 20°, all the reflected rays will be reduced by the same reflectivity factor. The reflectivity factor for all the power in the lobe should then be the same as that of a ray incident on a smooth seawater surface and normal to the surface.

A test of the soundness of this simple model of the scattering process was provided by measurements of the sea-surface temperature.[2] With 1- to 1.5-m waves, the radiant temperature of the sea computed using this simple model was higher than the measured radiant temperature by 0.7 K. The radiometer was a third-generation instrument with an accuracy of approximately 0.1 K (ref. 4–44).

The error is of the correct sign, if the model does not account for reflectivity outside the main lobe. The extra reflectivity not accounted for by the facet model (Kirchhoff approximation) will cause the model to predict a radiant temperature that is in error by $\Delta T = T_M \Delta P$, where T_M is the radiant temperature in the main lobe and ΔP is the fraction of the power scattered out of the main lobe. Then $\Delta P = 0.7/280 = 0.0025$. That is, 0.35 of the power is scattered into the main lobe (at 2.65 GHz), and 0.0025 of the power is scattered out of the main lobe. The total diffracted scattered power is then 21.5 dB below the main lobe power.

To clarify this rationale, note that maximum wave slopes lie between 10° and 20°, depending on sea state; therefore, the main lobe has a beamwidth of 20° to 40°. The ratio of the solid angle subtended by the main lobe (¼ rad) to the hemispherical solid angle subtended by the diffracted energy is 25 (or 14 dB). The average diffracted power density should then be down from the main-lobe power density by -21.5 dB $+(-14$ dB$) \approx -36$ dB.

Fortunately, Moore (ref. 4–45) gives the reflectivity of water near vertical incidence. The data are given for a lake rather than the sea, but they serve to estimate the magnitude of that reflectivity. Moore's data at 3.8 GHz show that the radar return is down approximately 35 dB at 30° from nadir. It then seems reasonable that the diffracted power density is approximately 36 dB down from the main-lobe power density in the case of the sea, thus showing that the radiometer results are consistent with the experimentally determined reflectivity patterns of the sea.

The preceding analysis also shows that energy diffracted out of the main lobe may be neglected in calculating the main-lobe pattern with little resulting error.

The measurement technique then consists of directing a radar beam straight down and

[2] Ho, W.; Hidy, G. M.; VanMelle, M. J.; and Love, A. W.: Radiometric Observations of Sea Temperature at 2.65 GHz. North American/Rockwell Space Center, Thousand Oaks, Calif., unpublished data.

moving it away from the nadir both along-track and crosstrack while measuring the magnitude of the radar return. To use these data for obtaining rainfall attenuation, an alternate expression for the radar return will be used that involves the directivity of the power reradiated from the surface and the illuminated surface area.

The two methods of received power calculations (radar cross-section analysis and target reflectivity pattern analysis) are compared in equations (4–23) and (4–24), where P_d is power density from radar antenna, P_{re} is power reradiated in radar direction, and P_{rec} is power received by radar. The radar cross-section analysis is

$$P_d = \frac{P_t G_t}{4\pi R^2} e^{-\alpha R} \qquad (4\text{–}23a)$$

$$P_{re} = \sigma \frac{P_t G_t}{4\pi R^2} e^{-\alpha R} \qquad (4\text{–}23b)$$

$$P_{rec} = \sigma \frac{P_t G_t A_r}{(4\pi R^2)^2} e^{-2\alpha R} \qquad (4\text{–}23c)$$

The target reflectivity pattern analysis is

$$P_d = \frac{P_t G_t}{4\pi R^2} e^{-\alpha R} \qquad (4\text{–}24a)$$

$$P_{re} = A_s G(2\phi) \frac{P_t G_t}{4\pi R^2} e^{-\alpha R} \qquad (4\text{–}24b)$$

$$P_{rec} = A_s G(2\phi) \frac{P_t G_t A_r}{(4\pi R^2)^2} e^{-2\alpha R} \qquad (4\text{–}24c)$$

where

P_t = radar transmitter power
G_t = radar antenna gain
R = radar range
α = attenuation coefficient
σ = radar cross section
A_s = illuminated surface area
A_r = radar antenna cross section

The reflectivity pattern of the surface is $G(\Psi)$, where $\Psi = 0$ on the main-lobe axis. When the radar beam is at depression angle ϕ, then Ψ along the line of direction to the radar is 2ϕ, as shown in figure 4–11.

It is assumed that the pattern rotates as ϕ changes, without changing shape. This holds true because, if the facet theory is accepted, the slope distribution of the sea will produce the same distribution of power around $\Psi = 0$, regardless of ϕ.

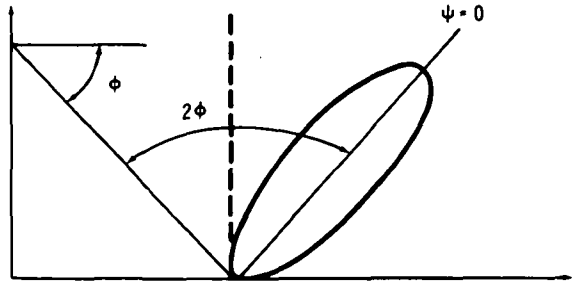

FIGURE 4–11.—Reflectivity pattern of the surface.

By definition, $\sigma = \sigma^\circ A_s$, where σ° is the target reflectivity. By setting equation (4–23b) equal to equation (4–24b) and canceling terms, one determines that $\sigma = G(2\phi)A_s$. Therefore, $\sigma^\circ = G(2\phi)$. In the special case of the radar looking at the nadir, $\Psi = 2\phi = 0$ and

$$\sigma^\circ = G(0) = \rho_{av} \frac{4\pi}{\Delta\psi^2} \qquad (4\text{–}25)$$

where ρ_{av} is the average reflectivity of the surface.

If the surface reflectivity ρ is unity and the surface is perfectly smooth, the beamwidth of the reflected power becomes the beamwidth of the illuminating antenna and

$$\sigma^\circ \rightarrow G_t = \frac{4\pi}{\Delta\phi^2} \qquad (4\text{–}26)$$

If for circular polarization, ρ is independent of Ψ over the range of incident angles and facet slopes under consideration, then the incident power density P_{inc} multiplied by the integral of $G(\Psi)$ over the hemisphere will be equal to simply ρP_{inc}; that is,

$$P_{inc} \int_0^{2\pi} G(\Psi)\, d\Omega = \rho P_{inc} \qquad (4\text{–}27)$$

where $d\Omega$ is the differential solid angle and

$$\int_0^{4\pi} G(\Psi)\, d\Omega \approx \int_{\Omega_a} G(\Psi)\, d\Omega = \rho \qquad (4\text{–}28)$$

where Ω_a represents the main lobe of the an-

tenna. This relationship is true even if $G(\Psi) \rightarrow G_t(\Psi)$ when the surface becomes smooth.

Then, the return power measured by the radar as it scans its beam around the nadir outside the main lobe can be written

$$P_r(\phi) = ka(\phi) G(2\phi) \exp (-2\alpha h \sec \phi) \quad (4\text{–}29)$$

where h is altitude and $a(\phi)$ is a resolvable element of area (depending on the radar antenna beamwidth $\Delta\phi$ and on range resolution Δr). Therefore

$$G(2\phi) = \frac{P_r(\phi) \exp (2\alpha h \sec \phi)}{ka(\phi)} \quad (4\text{–}30)$$

and

$$\int G(2\phi)\, d\Omega = \int \frac{P_r(\phi) \exp (2\alpha h \sec \phi)}{ka(\phi)} d\Omega = \rho \quad (4\text{–}31)$$

This is an integral equation which can be solved for α.

The preceding discussion presents only an outline of a possible measurement method. A thorough error analysis is needed to establish feasibility.

Once attenuation for the total path is known for a series of measurements (using fixed ground stations and the sea surface) for a large selection of rainfall rates and types, a calibration factor can be used to adjust the total attenuation measured by the radar. The calibration factor is adjusted so that the one-way and the radar attenuations agree statistically for that set of observational data.

Cross-Polarization for the Determination of Drop-Size Distribution and Melting Layer Height

Electromagnetic waves propagating through precipitation are depolarized by the nonspherical shape of the particles. At frequencies sufficiently high so there is an appreciable variation of the dipole moment as a function of orientation, the cross-polarization can be measured and used as an indicator of the type or size of precipitation particles. Typically, at frequencies of 9 GHz or higher, depolarization is sufficiently strong to be used for studying atmospheric precipitation effects.

Rain appears as an anisotropic medium to short-wavelength radio waves. Raindrops assume an oblate spherical shape as they fall, and their axes are oriented within a relatively small range of canting angles. Consequently, a differential phase shift and attenuation exists between horizontally and vertically polarized fields, and this differential refractivity causes a change in polarization along the path. A radar, viewing a rain cell at a wavelength such that the cell is penetrated, has returns that depolarize as a function of the intensity and type of precipitation.

The strong dependence of radar echo on drop diameter enables a multiwavelength radar to measure parameters of the drop-size distribution. Larger drops are more oblate than smaller drops. Therefore, the ratio of the cross-polarized return provides an additional measure of the drop-size distribution. In effect, the number of measurements is doubled, allowing some determination of the departure from an exponential distribution to be assessed.

For a medium containing particles with a number density n, the attenuation coefficient is

$$k = k_0 \left(1 + \frac{2\pi n}{k_0^2} \mathcal{R}eF_s\right) \quad (4\text{–}32)$$

where F_s is the parallel-polarized forward-scatter amplitude and $k_0 = 2\pi/\lambda$. Considering the particles as dielectric oblate spheroids having a vertical semiaxis c and a horizontal semiaxis a, the difference in index of refraction for vertically and horizontally polarized waves is

$$\Delta k = k_0 \left\{ n \frac{4\pi a^2 c}{3} \left[\frac{\epsilon - 1}{(\epsilon - 1) a^2 c I_c + 2} - \frac{\epsilon - 1}{(\epsilon - 1) a^2 c I_a + 2} \right] \right\} \quad (4\text{–}33)$$

where ϵ is permittivity and I_c and I_a are integrals for the oblate spheroid (ref. 4–46). Using a Laws and Parsons drop distribution and the drop ellipticity relation of Spilhaus (ref. 4–47), the differential phase change per unit length through 50-mm/hr rainfall at 3-cm wavelength is approximately 7×10^{-5} rad/m. For the two-way propagation through a 9-km rain cell, the calculated phase change between horizontal and vertical polarization components is approximately 70°.

The previous discussion indicates that the use of circular polarization is advantageous for meteorological measurements by satellite radar. The principal return is received by transmitting circular polarization and receiving the opposite sense. Measurement of the two senses of circular polarization could be made by an appropriate combination of two linear polarization returns. In any event, two receivers are needed.

The depolarization of the radar return from a cell within a region of precipitation is produced by two causes. The first cause is the propagation through the anisotropic medium, with its different attenuation and refractivity to horizontal and linear polarization. The second cause is the variation in radar cross section with polarization caused by particle ellipticity in the particular cell being observed. These causes can be quantified in a straightforward manner. The depolarization ratio is the ratio of received power having the same sense of circular polarization as the transmitted power to the power received with the orthogonal-sense circular polarization. The ratio is

$$\chi(z)=\left|\frac{1-C(z)\,\exp\left(-j2\int_0^z \Delta k\,dz\right)}{1+C(z)\,\exp\left(-j2\int_0^z \Delta k\,dz\right)}\right|^2 \qquad (4\text{–}34)$$

where z is the distance from the radar to the cell being observed, $C(z)$ is the polarization reflection ratio at the cell, and j is equal to $\sqrt{-1}$. For a spherical particle, C is unity.

Measurement of χ as a function of z (a relative power measurement) thus affords a determination of the complex index of refraction. From this information, and assuming a relationship of drop ellipticity with size, one can determine the parameters of the drop-size distribution.

The choice of frequencies of operation is consistent with the earlier discussion of drop-size distribution using a multiwavelength radar. The difference in dipole moment is appreciable where the path attenuation is significant. In fact, the depolarization measurement can be used in the same manner as the attenuation measurement in a two-wavelength determination of drop-size spectrum. This additional constraint permits the determination of the three parameters in a three-parameter drop-distribution model. This determination permits closer approximation of the actual drop-size distribution.

To show this effect, a depolarization parameter $p_d(\lambda)$ is defined such that

$$P_{2t}=[1-\exp\,(-\int p_d(\lambda)\,dl)\,]P_{1i} \qquad (4\text{–}35)$$

where P_{1i} is the incident power in polarization 1, P_{2t} is the transmitted power in polarization 2, and l is the path length. The parameter P_{2t} is related to the scattering matrix of the raindrop. The expression for l, analogous to equations (4–30) and (4–31), is

$$p_d(\lambda)=\sum_D Q_{12}(D,\lambda)N_D \qquad (4\text{–}36)$$

where attenuation Q_{12} is derivable from the scattering matrix. Note that $p_d(\lambda)$ goes to zero as λ approaches infinity.

If it is assumed that both senses of circular polarization are attenuated equally and reflected equally by the resolvable element of range at range R, the ratio of powers F_p in the two polarizations at range R (at the attenuating depolarizing wavelength) is

$$F_p(R)=1-\exp\left[-\int_0^R 2p_d(\lambda,R)\,dR\right] \qquad (4\text{–}37)$$

and at range $R+\Delta R$ is

$$F_p(R+\Delta R) = 1 - \exp\left[-\int_0^R 2p_d(\lambda, R)\, dR - 2p_d(\lambda, R)\, \Delta R\right] \quad (4\text{–}38)$$

Solving for $\exp[-2p_d(\lambda, R)\Delta R]$, one obtains

$$\frac{1-F_p(R+\Delta R)}{1-F_p(R)} = \exp[-2p_d(\lambda, R)\, \Delta R] \quad (4\text{–}39)$$

Thus, the value of the depolarization parameter at range R is derived in terms of the measured quantities $F_p(R)$ and $F_p(R+\Delta R)$. The three parameters in a three-parameter drop-size model must then be set to satisfy equation (4–36) as well as equations (4–30) and (4–31).

Measurements of cross-polarization can also be used to assess the melting layer. The strong depolarization produced in the melting layer is caused by the irregular shapes of particles as they melt and re-form. Indications are (ref. 4–48) that the polarization properties of the melting layer, when added to the principal-polarization echo-strength data, permit a good assessment of the layer depth. Experimental measurements have shown the strong polarization properties of the melting layer. Hendry and McCormick (ref. 4–49), using a dual-channel-polarization diversity radar operating at 1.8-cm wavelengths, observed the depolarization in rain, snow, and the melting layer.

By transmitting circular polarization and receiving both senses of circularly polarized returns, Hendry and McCormick observed a relative level of cross-polarization approximately 10 dB below the main returns. This level is approximately 20 dB greater than the cross-polarization of moderate snow and corresponds to the cross-polarization of rain at rates of approximately 50 mm/hr. Note that these levels are ratios of returns and not the absolute levels of the returns. The melting level can be distinguished from rainfall because the cross-polarization level remains approximately constant with depth, whereas in rainfall the cross-polarization increases with depth. Thus, a high depolarization that is constant with depth is an indicator of the melting layer, and an increasing depolarization is a characteristic of rainfall. The rate of increase of the cross-to-copolarization power is a function of the rainfall rate.

Implementation of polarization measurements does not impose new or unusual requirements on the satellite radar. The antenna must be designed to have good polarization separation, with two output channels having essentially identical radiation patterns. A typical requirement for the antenna-integrated cancellation ratio for each channel is 26 dB; this value is representative of good antenna design. The cross-polarization ratio of 5-mm/hr rainfall at 1.8 cm is under 20 dB; therefore, measurements at this rainfall rate should be possible with good antenna control. By using a dual-polarization feed and two receivers, the radar can be used to produce any polarization desired for an experiment.

The use of polarization measurements extends beyond the inference of meteorological phenomena. Circular polarization is widely used for weather clutter cancellation in the navigation and traffic control radars for marine and air services. There is a need for much more data, particularly data on a global scale, that show the statistics of depolarization. From a comprehensive measurement program, enough data could be extracted to develop reliable models for radar return depolarization so that radar designers and users could take appropriate account of weather effects on the subclutter visibility that can be expected from circular polarization.

Using Doppler Techniques to Measure Drop-Size Spectra From a Geostationary Satellite

A geostationary satellite has the capability of measuring the Doppler spectrum of precipitation resulting from differential fall rate. Because this satellite is almost stationary with respect to the Earth, the satellite or the Earth motion produces only a very small Doppler shift. If such a Doppler radar

observes precipitation, there is therefore practically no smearing of the fall-rate spectrum, as in the case of lower orbit satellites (such as discussed in the section entitled "Satellite-Borne Radar With Doppler Capability").

The drop-size distribution and liquid-water content cannot be directly inferred from the fall-rate spectrum because of the component of the wind vector projected on the line of sight. However, if the reflectivity of the rain is also measured, both the drop spectra and wind component can be obtained. This determination is accomplished by varying the assumed wind-velocity component and calculating the drop-size distribution that would be present for each assumed velocity. Only one assumed velocity will yield a size distribution for which the reflectivity is the observed reflectivity. Then, the wind component, size spectrum, and liquid-water content are known.

This procedure must start at maximum echo height. Then, as the size distribution of each increment in range is computed, the corresponding attenuation for the cell can be calculated. The total attenuation from maximum echo height to each successive cell can then be used to obtain the true reflectivity from the measured reflectivity. This technique is subject to the same restrictions on swath width as discussed elsewhere in this report.

Cirrus Cloud Detection

Clouds are generally not detected by ground-based microwave radars. Exceptions are very dense cumulus clouds and cirrus clouds. As an example, figure 4–12 shows a cirrus cloud detected on a high-sensitivity S-band radar. In this photograph, the cirrus cloud extends between 6 and 12 km in altitude and between 10 and 86 km in range. The inside of the cloud appears black because of the "slicing" circuitry that was used to obtain a measure of reflectivity of the clouds. The strongest return in the cloud was in the 76- to 79-dBm slice, which corresponds to approximately 20 dBZ ($dBZ = 10 \log_{10} Z$).

Definitive results from radar studies of cirrus clouds are not available, although tools for such research are presently in existence. The fact that cirrus clouds are visible on sensitive radar comes from the rather large size of the ice particles. Jones (ref. 4–50) gives the following expression for the density of water droplets in ice clouds:

$$n(D) = [-2.67 M_t^{-1/3}(D - 0.25)] \times 10^{4.1} \quad (4\text{–}40)$$

for droplet diameters ≥ 0.25 mm, where M_t is total ice content in grams per cubic meter. Note that these particles are in the millimeter region, compared to liquid cloud drops that have peaks in their distributions at less than 10 μm. Although further research is required in this area, satellite-borne ultrasensitive radar might well be used to study the occurrence, density, and thickness of cirrus clouds.

The multiwavelength radars discussed in this section have an obvious applicability in cirrus detection. Water clouds attenuate microwave frequencies much more than ice clouds. As an example, at approximately 263 K and for $\lambda = 0.9$ cm, the attenuation is 1.2×10^{-3} dB/km/g/m^3 compared to 3×10^{-3} dB/km/g/m^3 for water and ice, respectively, for one-way paths. With the difference in attenuation being two orders of magnitude, it may be possible to distinguish between water and ice clouds. Similarly, this technique might also be applied in distinguishing between rain and snow.

SATELLITE-BORNE RADAR WITH DOPPLER CAPABILITY

In the past few years, as previously mentioned, satellites have provided meteorologists with day-and-night monitoring of cloud systems on a global scale. Geostationary satellites are currently observing cloud formation over large regions on Earth, and the observations are frequently repeated so that the movement of cloud systems can be detected and measured. Orbiting satellites operate from a much lower altitude, are capable of better resolution, and can also carry a greater variety of experiments.

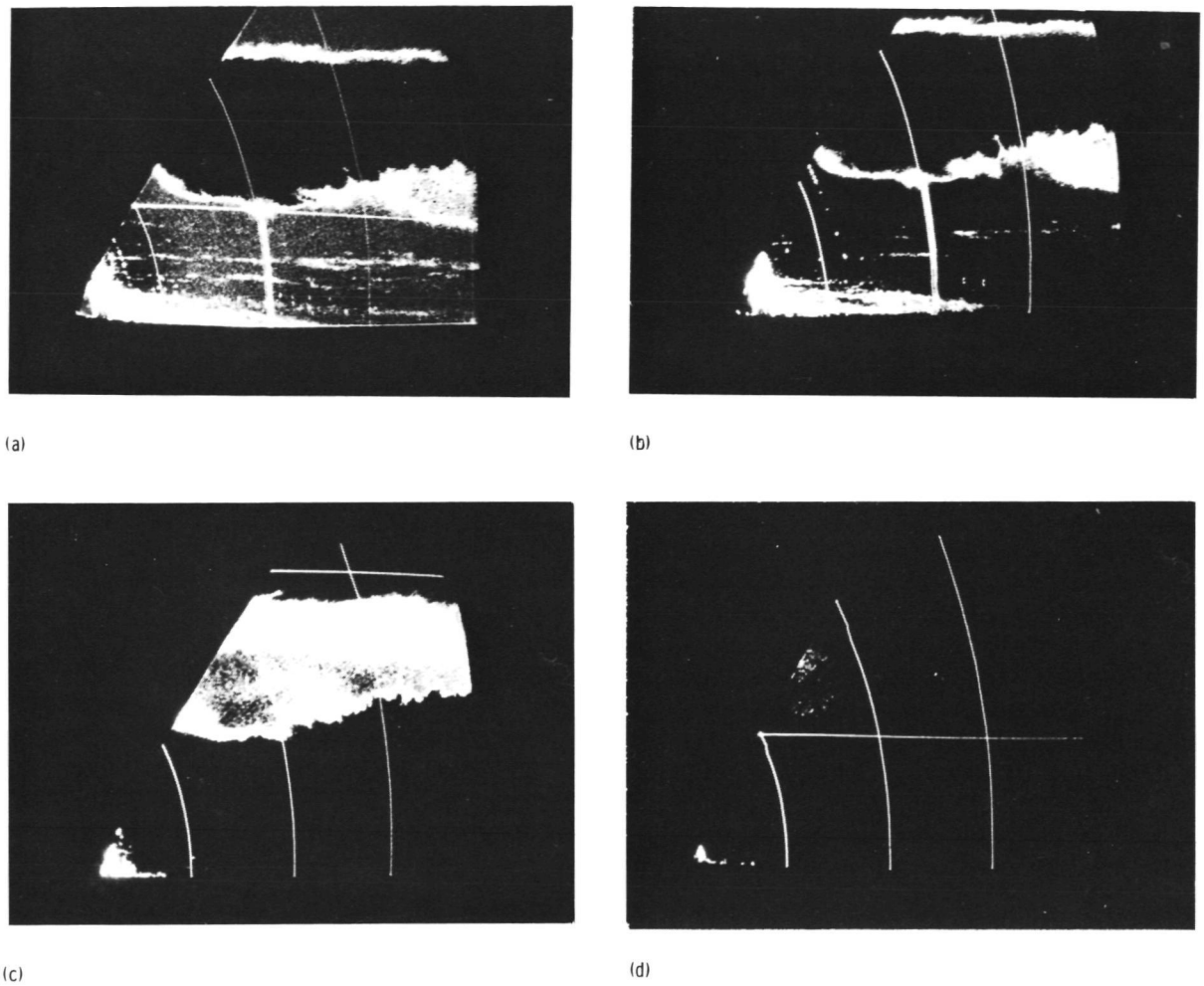

FIGURE 4–12.—Cloud and clear-air echoes with a slicer azimuth of 270°. (*a*) Window: 100 to 103 dB. (*b*) Window: 94 to 97 dB. (*c*) Window: 76 to 79 dB. (*d*) Window: 61 to 64 dB.

Indeed, meteorological satellites are now widely accepted as indispensable tools for the monitoring of cloud and cloud-top temperature with infrared sensors either from low-altitude orbits with substantial swath or from a geostationary orbit.

Passive microwave radiometers, which are now being flown on several Nimbus experiments, have also demonstrated excellent operational capabilities. However, such systems do not have the unique ranging capability of an active microwave system (radar).

None of the existing meteorological satellite capabilities include the monitoring of vertical and horizontal distribution of precipitation inside large meteorological systems (hurricanes; intertropical convergence zones; large, persistent squall lines; etc.), which could be achieved by use of a satellite-borne radar.

The constant day-to-day monitoring of the precipitation system associated with a hurricane over regions where there are no ground-based or shipborne radars is certainly one of the most significant examples of the use-

fulness and uniqueness of the satellite-borne meteorological radar.

Also, the observation of severe storm continental mesoscale systems could improve severe storm forecasts and warnings. These systems tend to lie along extended bands (squall lines) but are usually contained within a zone 200 to 400 km ahead of the cold front surface position (ref. 4–11). The squall-line zones can sometimes extend for more than 1400 km along the front and their duration can exceed 1 day, although the squall lines themselves have lifetimes of several hours and lengths of less than 300 km. It should be noted that even in the continental United States, where radar observations can easily be made, the monitoring of such precipitation systems over areas of a size comparable to that provided by satellite coverage would require the difficult compilation of data provided by a large number of ground-based radars.

A comprehensive study (ref. 4–22) on the feasibility of satellite-borne radars for meteorological observations was done by Stanford Research Institute under NASA sponsorship. This study concluded that such a facility had very little practical value for the mesoscale study of precipitation mainly because of the limited coverage and low sampling rate allowed by that system. However, the observation of large-scale, persistent meteorological features by satellite does not require the time and space resolution that is common to ground-based radars observing this type of weather over much smaller areas. This section will be mainly concerned with the possible use of Doppler radar techniques for the monitoring of windfields inside such precipitation systems, using precipitation particles as tracers for air motion.

In the case of a satellite placed in a low-altitude orbit, the use of Doppler radar techniques is made difficult by the very large groundspeed of the satellite. The major effect is a natural spread in the Doppler because of the different radial velocities of scatterers in various parts of the beam. It is evident that this effect is decreased for narrow beams and that it is a function of the beam scanning angle and direction. As an example, using parameters applicable to the proposed system, one finds that the maximum standard deviation of the Doppler spectrum due to this effect is 6 m/sec for a satellite groundspeed of 6.9 km/sec.

It must be noted that the satellite speed combined with the conical beam scan (which will be proposed in this section) also constitutes a useful capability, because the same target will be "seen" from different directions for which the target speed will result in different Doppler velocity components. Because this report will consider the possible application of Doppler radar methods for the measurements of atmospheric motion, it is appropriate to present the following brief review of the subject.

Doppler Radar Methods

Doppler radars provide a means for monitoring the radial velocity of targets (approaching or receding motion). If atmospheric targets are moving at the surrounding airspeed, such as in the case of precipitation particles, the method can easily be extended to the measurement of atmospheric air motion. Precipitation particles, or manmade targets ("chaff"), released in the atmosphere are considered as tracers for the air motion.

A single Doppler radar provides observations and mapping of the radial velocities of precipitation particles only. The information has the form of a spectrum of radial velocities that is produced by the distribution of particle velocities inside the scattering volume. In the case of turbulence, the spectrum is influenced by the space variability of the motion. In this case, the size of the scattering region controls the spread or variance of the Doppler spectrum; that is, the ability of the radar to effectively resolve these motion scales. This method has been used for observing the vertical velocities of precipitation particles with the radar beam pointed vertically so that particle size or air vertical velocity can be derived from the observed data. For example, cloud physics pa-

rameters, such as growth by deposition and riming, have been observed in winter storms. Horizontal wind can be probed by a method involving complete 360° scanning of a tilted radar beam, essentially providing different radial velocity components of the same wind, if the radar is inside a widespread precipitation system where the wind is horizontally homogeneous. These techniques are not applicable to the study of the structure and kinematics of localized convective storms, which basically require the simultaneous use of several Doppler radars installed at different locations and observing the same storm. In this method, the radar beams cooperatively scan the same region and thereby provide several radial components of the particle velocities, so that two- or three-dimensional velocity can be observed (ref. 4–51).

A dual-Doppler-radar system that provides two-dimensional velocity estimates is the first and most important step in this direction. In this method, two Doppler radar beams scan a common atmospheric region, a tilted plane intersecting the line joining the two radars. A set of such planes provides three-dimensional scanning of the region of interest.

At any point in a tilted plane, two different radial velocity components can be observed from the radial velocity samples acquired by the two radars. Two noncollinear radial velocity estimates can then be used to compute the two-dimensional velocity vector at that point on the plane.

Removing the contribution due to terminal velocity from the observed radial velocities, and assuming again that particles are moving at the airspeed, leads to the expression of the components u' and v' of the three-dimensional air velocity projected on the tilted plane. Inspection of the vector windfield can reveal patterns of convergence and vorticity of the observed motion field that are useful for descriptive modeling of storm kinematics.

If the convergence of the motion field in the tilted plane is computed, then the velocity component w' normal to the plane can be evaluated from the following equation of continuity for a noncompressible fluid:

$$\frac{\partial u'}{\partial x'} + \frac{\partial v'}{\partial y'} + \frac{\partial w'}{\partial z'} = 0 \qquad (4\text{–}41)$$

In this equation, x' and y', respectively, are rectangular coordinates parallel and perpendicular to the baseline. The use of the equation of continuity, which relies on steady-state kinematic conditions in convective storms, is very important because it virtually removes the need for a third radar, which would bring more complexity. The dual-Doppler-radar method has been presented and discussed in several papers (refs. 4–51 to 4–54), and an example of the motion fields observed by this method is shown in figure 4–13.

It must be noted that, although single-Doppler-radar measurements yield limited information on wind, fields of mean Doppler velocities may generate characteristic features (signatures) that can, under certain circumstances, be related to significant meteorological events, such as vortex motion (ref. 4–55).

An example of how a display of single-Doppler velocity fields can be used to infer mesocyclone characteristics is shown in figures 4–14 and 4–15, where a PPI sector

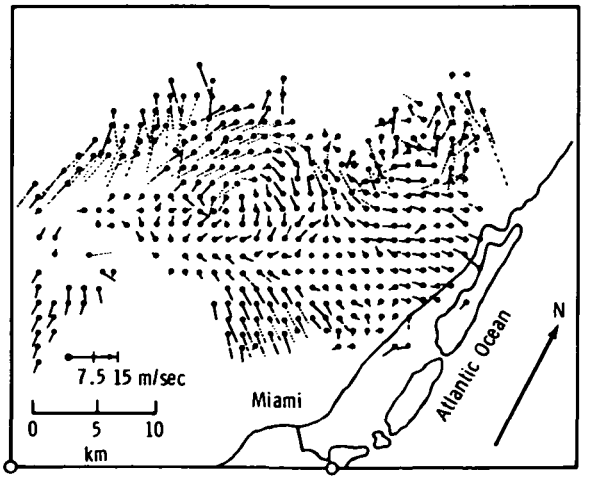

FIGURE 4–13.—Example of a motion field observed with a dual-Doppler-radar system inside a convective storm; plane tilt, 14°.

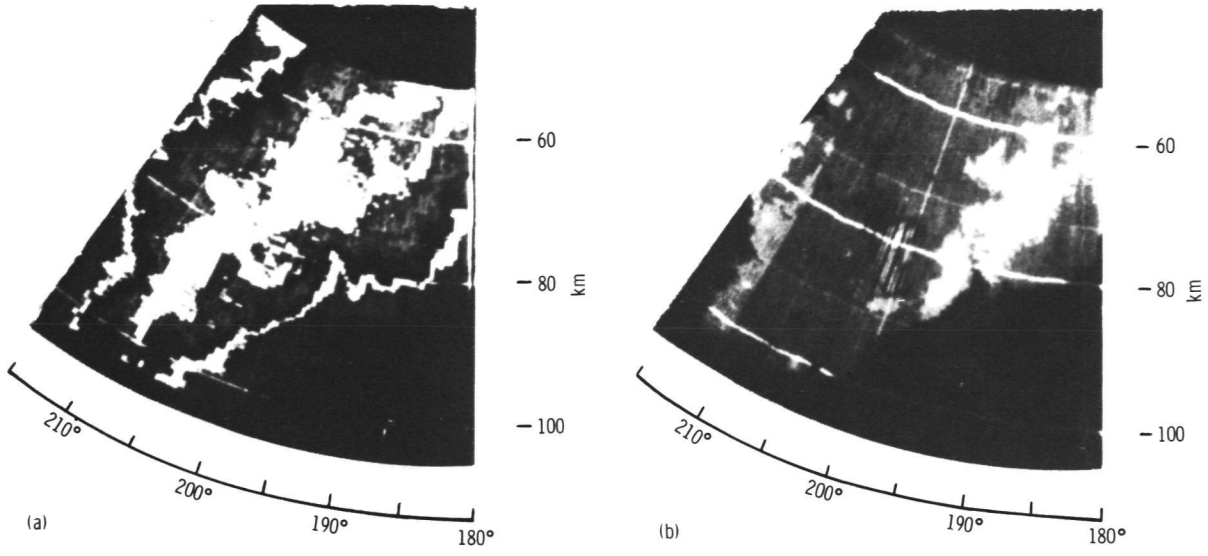

FIGURE 4–14.—Plan-position-indicator reflectivity and isodops. The elevation angle is 1.9°; range marks are at 60, 80, and 100 km. Reflectivity categories are dim (<21 dBZ), bright (21 to 31 dBZ), black (31 to 44 dBZ), dim (44 to 57 dBZ), and bright (>57 dBZ). Velocity categories are dim (<13 m/sec), bright (13 to 21 m/sec), and brightest (>21 m/sec). Positive radial velocities are angularly strobed. Mesocyclone-type signature between 193° to 203° and 75 to 90 km. (*a*) Plan-position-indicator reflectivity. (*b*) Plan-position-indicator isodops.

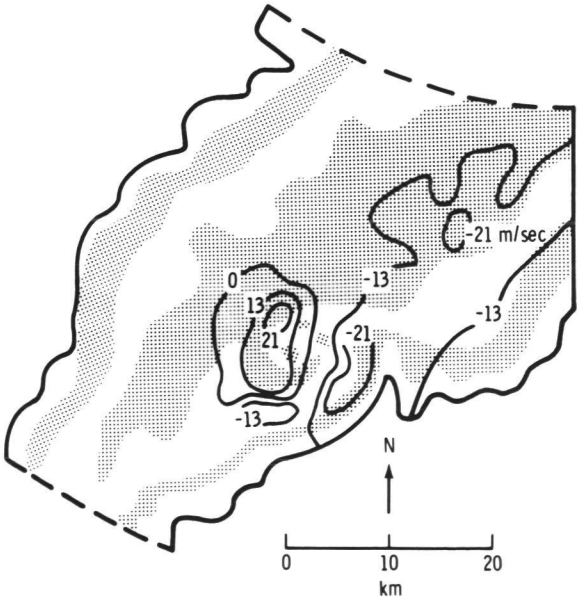

FIGURE 4–15.—Overlay of figure 4–14 reflectivity and radial velocity fields; tilt, 1.9°.

displays constant Doppler velocities (isodops) and constant echo power resolved with a 10-cm Doppler radar (0.8° beamwidth, 1-μsec pulse width). In figure 4–14(*b*), PPI trace brightness is used to indicate Doppler magnitude in the form of isodops. Figure 4–14 shows the echo pattern obtained simultaneously with the radial velocity field. Note the "hooklike" feature, which suggests mesocyclonic circulation. The isodop and reflectivity fields are overlayed in figure 4–15 to facilitate pattern comparison. It can be shown that circularly symmetric cyclonic motion forms a symmetric couplet of closed isodops with an equal number of lines encircling positive and negative velocity maximums. The nearly symmetric isodop pattern (fig. 4–15) indicates cyclonic rotation consistent with the reflectivity pattern. It can be shown that a signature pattern for circularly symmetric convergence is identical to a vortex pattern, but rotated by 90°. The apparent reflectivity spiral in the figures suggests convergence, a view supported by the clockwise angular displacement of isodop maximums about the vortex center.

In short, it is noted that single Doppler isodop displays may indicate storm structure, and it is expected that displays of satellite-derived radial velocity could likewise exhibit similar dynamic features.

Although pulse Doppler radars have been used extensively for research, there is no radar operated by the National Weather Service that is equipped for Doppler measurements. However, methods for using single Doppler radars are now being effectively developed so that the operational use of the Doppler radars may become effective in the next few years.

Doppler Radar Signal Processing

The velocity information contained in the Doppler radar signals can be expressed by a spectrum of speed related to the distribution of radial velocities of the precipitation particles in the pulse volume. The spectrum width is due to the actual statistics of precipitation particle velocities; however, in the case of a moving platform, substantial smearing of the spectrum can also originate from the change of radial velocities throughout the finite angular size of the radar beam. Such smearing is overwhelming in the case of a fast-moving radar, so that spectrum width may have little meteorological significance. However, the spectrum first moment or "mean Doppler" can contain meteorologically significant information. This estimate of the spectrum first moment can be obtained by simple processing systems, such as the signal covariance estimator, which is now used in ground-based Doppler radar applications (refs. 4–53 and 4–54). Also, quantitative mean Doppler estimates of slightly larger variance can be obtained by a simple device measuring the signal phase change (ref. 4–56).

The covariance estimator allows the tracking of the mean Doppler through any of the frequency ambiguity regions associated with the signal sampling rate (radar pulse repetition rate). Moreover, it is not biased by the occurrence of noise, which only increases the uncertainty or variance of the estimate. The only limitation of the covariance estimator for an accurate mean Doppler measurement occurs when spectrum width approaches the spacing (i.e., PRF) between frequency ambiguity lines.

Satellite-Borne Radars

An important limitation in the application of ground-based radar measurements to mesoscale and global-scale studies is the lack of mobility and the very limited coverage of the radars. The installation of radar systems aboard an airplane allows observations over much larger regions on Earth. If such methods for monitoring precipitation and possible atmospheric motion are implemented aboard an orbiting satellite, observations over the entire Earth will be provided.

The applicability of Doppler radar techniques to satellite instrumentation is made difficult by the high groundspeed of the satellite, which causes a Doppler frequency shift much larger than that due to the ground velocity of precipitation particles moving with the atmospheric wind.

In the case of a vertically pointing beam for which the axis is perpendicular to the satellite trajectory, the satellite motion does not produce a mean Doppler shift, but results in a smearing of the Doppler frequencies because of the finite size of the beam inherent in any antenna system. Note that it has been stated earlier that only the smearing of the spectrum limits the accurate recovery of mean Doppler because the velocity ambiguity region can be specified by beam position and satellite speed.

The limited coverage of a vertically pointing beam carried by an orbiting satellite will scarcely be acceptable as the means for probing large meteorological systems. It is indeed necessary that the satellite provide complete coverage on the Earth surface, at least in regions that are significant in terms of occurrence of precipitation systems. That coverage must be of the same nature as the cloud coverage provided by the infrared and visible sensors flown in orbiting satellites (such as NOAA–2 and NOAA–3) or geo-

stationary satellites (such as ATS–3 or GOES).

This report presents an example of two possible methods that would provide satisfactory solutions.

Doppler Radar Wavelength Selection

To determine the characteristics of a Doppler radar, it is necessary to specify certain meteorological objectives. First, assume a range resolution of 1 to 2 km and a 2-km "angular" resolution to provide meteorologically useful data on mesoscale systems and a vertical velocity resolution of 1 m/sec.

Range and velocity can be simultaneously resolved with a pulse Doppler radar. Velocity resolution ΔV is related to wavelength λ and dwell time $N_s T_s$ as

$$\Delta V = \frac{\lambda}{2N_s T_s} \qquad (4\text{–}42)$$

where N_s is the number of echo samples used to derive a mean Doppler estimate and T_s is effectively the sample spacing (i.e., pulse repetition time). The maximum velocity V_m that a pulsed Doppler radar can unambiguously resolve is given by

$$V_m = \pm \frac{\lambda}{4T_s} \qquad (4\text{–}43)$$

Velocities in excess of V_m will result in Doppler spectrum aliasing, so that the mean Doppler velocity estimates may pass discontinuously from $-V_m$ to $+V_m$ for two adjacent radar sample volumes. However, by assuming spatial continuity of velocity, these ambiguities can be resolved, provided that a mean velocity at an initial location is correctly identified. To remove range ambiguities, T_s must be sufficiently large so that all echoes associated with one transmitted pulse are received before the echoes associated with the following pulse. The value T_s is given by

$$T_s = \frac{2R_m}{c} \qquad (4\text{–}44)$$

where R_m is the range to the most distant target. Combining equations (4–43) and (4–44)

$$\lambda = \frac{8R_m V_m}{c} \qquad (4\text{–}45)$$

where c is the velocity of propagation. Satisfying simultaneous requirements of large V_m and R_m necessitates long wavelengths. However, because the wavelength must be kept small to maintain good angular resolution with reasonable antenna diameters, R_m and V_m must be limited to the smallest acceptable values. However, to achieve an accurate mean velocity estimate, $2V_m$ should be large compared to the Doppler spectrum width so that there is no significant folding bias. For low-orbiting side-looking radar moving at a groundspeed of 7 km/sec and having 0.3° beamwidth, the 6-dB velocity spectrum width will be approximately 34 m/sec. A value of $2V_m = 75$ m/sec will provide the requisite accuracy, assuming precipitation plus ground clutter targets would be received over a range interval of approximately 55 km (fig. 4–16). Therefore, substituting $R_m = 55$ km and $V_m = 37.5$ m/sec into equation (4–45) yields $\lambda = 5.5$ cm for the

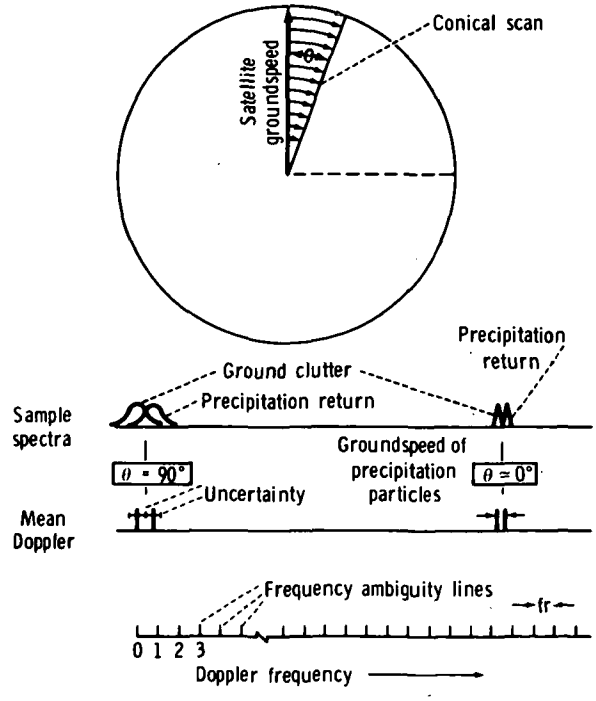

FIGURE 4–16.—Variation of the Doppler spectrum position and width with the scan angle θ.

minimum wavelength necessary to eliminate range ambiguity within the spatial limit of R_m. Thus, a minimum wavelength of 6 cm appears acceptable for satellite-pulsed Doppler operation.

In addition to Doppler considerations, the choice of the operating wavelength always may be conditioned by a compromise between the contradictory requirements of (1) narrow beams with practical-size antennas and (2) acceptable penetration of the radar signals in the precipitation systems. In this preliminary investigation, it appears that a decrease of the wavelength below X-band (3.2 cm) drastically increases the attenuation of the radar signals and therefore reduces the penetration of the signal and the significance of the quantitative data. On the other hand, a wavelength longer than 5 or 6 cm no longer improves the signal penetration performance significantly, and yet does result in an increased antenna size to meet the same angular resolution requirements.

The optimum wavelength lies somewhere between 3 and 5.6 cm. At a 3.2-cm wavelength, the beamwidth provided by a 12-m dish is 0.2°, and the two-way attenuation in a 15-km path in a 25-mm/hr rainfall is 13 dB. For the same conditions, but at a 5.6-cm wavelength, the beam size is 0.3°, and the attenuation becomes 2.6 dB, which is substantially less than in the 3-cm-wavelength case. It must be noted that, in the case of Rayleigh scattering, and neglecting attenuation, the sensitivity of a 3-cm-wavelength radar with respect to a 5.6-cm-wavelength radar is improved by 5 dB for the same angular resolution and overall radar characteristics.

A continuous-wave (CW) Doppler radar has no unambiguous velocity limit, and the maximum resolvable velocity is dictated by receiver bandwidth. Equation (4–42) applies equally well to a CW Doppler, except that there is continuous transmission during the dwell time $N_s T_s = T_{dw}$. For sufficiently small λ, T_{dw} can be made sufficiently small without changing ΔV so that the entire transmission can occur in a time that permits range resolution equivalent to that of a pulsed Doppler (i.e., 1 km). Solving equation (4–42) for λ, with $T_{dw} = 6.7$ μsec, yields $\lambda = 13$ μm.

Thus, a CW CO_2 Doppler radar (i.e., $\lambda \approx 10$ μm), transmitting for a duration of 6.7 μsec, should provide a velocity and range resolution of 1 m/sec and 1 km, respectively, and a Doppler radar at either of two wavelengths (6 cm and 10 μm) must be considered. It is interesting to note that wavelengths between these two limits would not meet the requirements of resolution without ambiguities.

Low-Altitude Orbit Satellite

The capability of a low-orbit satellite can be compared to NOAA–2 and NOAA–3 observational capabilities, which provide monitoring of large-scale time-persistent precipitation systems. With a Sun-synchronous polar orbit, the satellite acquires observational data for approximately noon or midnight at any point on Earth.

The low-altitude orbiting satellite method presented here is associated with difficult technological problems in extracting the Doppler velocity information from the backscatter signal, but it seems to be the only practical answer to a complete Earth coverage with acceptable resolution.

Low-altitude orbiting satellites are generally flown in an inclined (polar) orbit. This type of orbit provides excellent coverage in tropical regions where large, time-persistent meteorological systems occur. This section discusses a possible application based on the use of a circular quasi-polar orbit with a 58° inclination angle. The satellite altitude is 556 km with an orbit period of 1.6 hr. The angle of inclination of 58° [3] is chosen to maximize the latitude to which complete Earth surface coverage is obtained. In the example discussed here, the radar scans every surface region between ±68° latitude at least once in 12 hr (fig. 4–17).

The swath coverage across the orbital trajectory is obtained by rotating a tilted nar-

[3] A Sun-synchronous orbit could also be accepted.

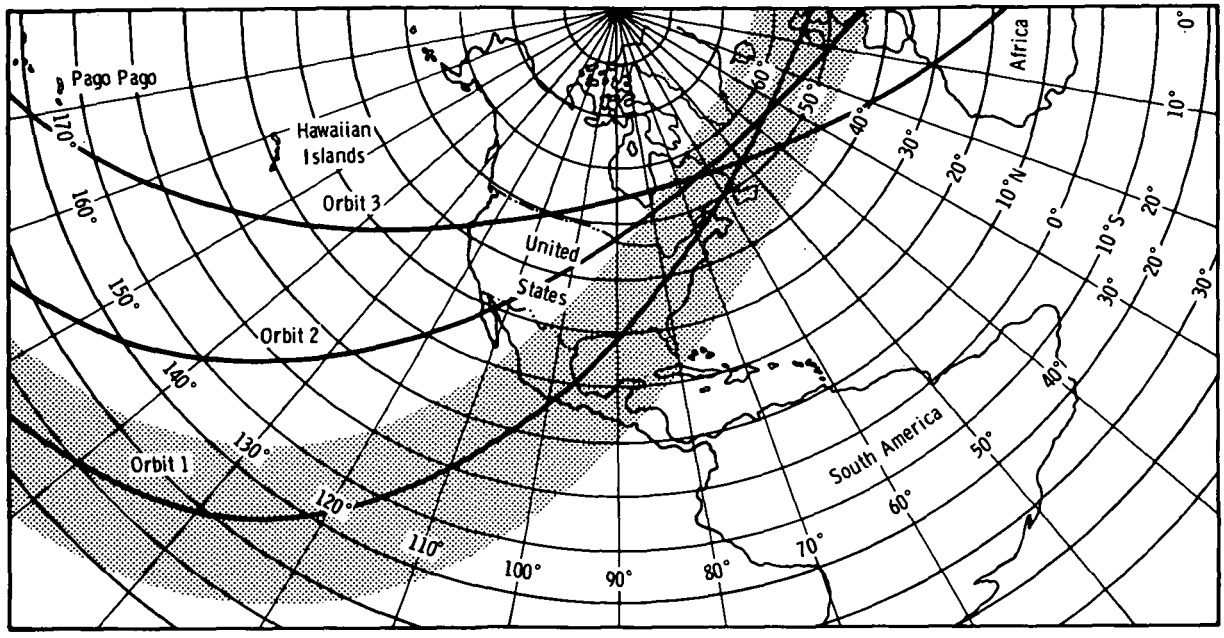

FIGURE 4–17.—Example of radar coverage available from an orbiting satellite at an altitude of 556 km. The orbit is quasi-polar with an inclination angle of 58°. The swath coverage is obtained by spinning a satellite carrying a tilted beam about a vertical axis.

row antenna beam around a vertical axis. The total swath width, which is approximately 2000 km, is obtained with a beam nadir angle of 60°. The configuration of the satellite in orbit and the swath geometry are shown in figure 4–18.

In the case of a pulse radar and an antenna radiation pattern free of any side lobes, the expected radar return is indicated in figure 4–19. There is a region contaminated by the ground or sea clutter that increases with the beam size. If the beam size is too large, the ground clutter occupies a substantial range interval; and the beam is no longer filled by the atmosphere in the "ground clutter free" part of the return. The maximum beam size that still allows substantial beam tilting for atmospheric observation can be determined as a function of the cross-swath range and the altitude h of the satellite, or the grazing angle γ.

For small beams, range gating of the radar signals in the range interval where only atmospheric targets occur will provide an effective means for probing the horizontal and vertical distribution of atmospheric targets (fig. 4–19). The process involved in range gating effectively selects scattering regions controlled by the radar pulse width. Small grazing angles, such as presented here (20°), favor horizontal resolution; the vertical resolution is controlled mainly by the beam size. With a 0.3° beam, a 20° grazing angle, and a 1000-km slant range, the vertical resolution is approximately 5 km; and, because of beam tilt, the horizontal resolution in the direction of the beam is approximately 2 km. The range gating will not affect the range resolution across the beam, which is still controlled only by the beam size.

However, the relationship between the mean altitude and horizontal position of the range gates depends on the beam tilt and limits complete atmospheric coverage. The simultaneous use of several contiguous, narrow beams (which is proposed later) can improve the coverage capability.

If there are no side lobes in the radiation

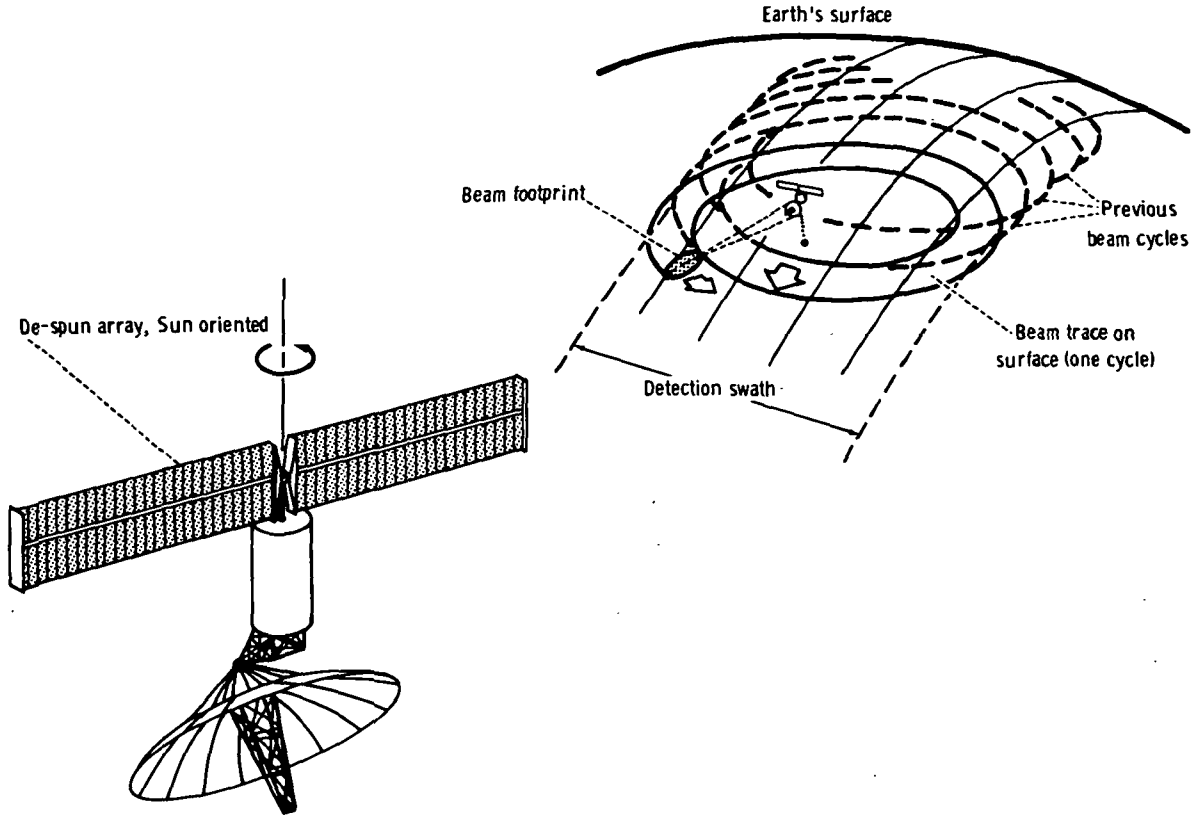

FIGURE 4–18.—Illustration showing the swath of an antenna producing beams that rotate about a vertical axis. The beam footprint is actually composed of a set of adjacent beams distributed radially.

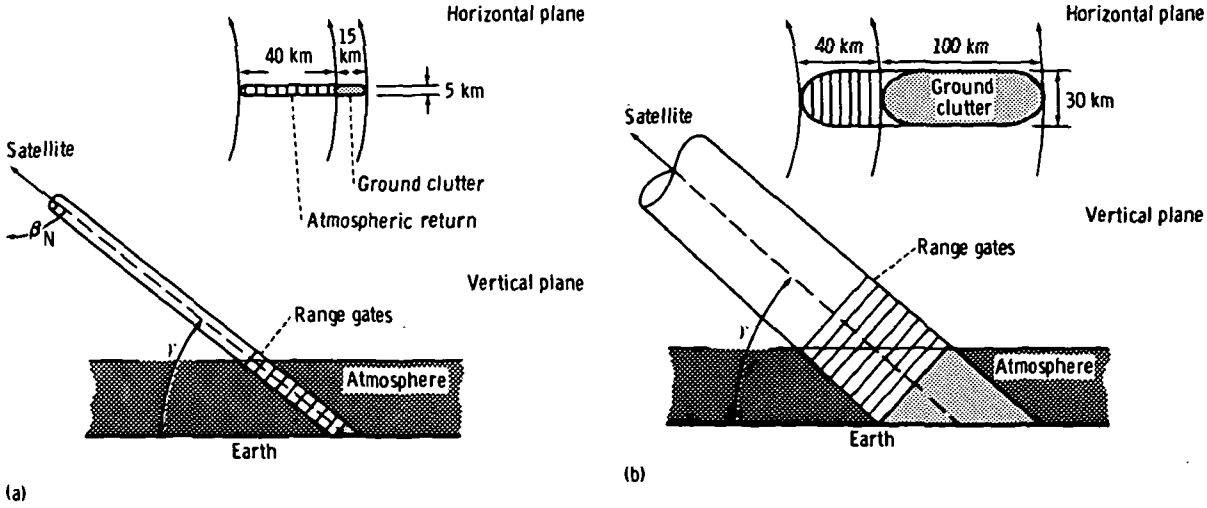

FIGURE 4–19.—Influence of the beam size on the importance of ground clutter and the filling of the beam by atmospheric returns. (*a*) Narrow beam (0.3°). (*b*) Wide beam (2°).

pattern, no backscattering is received between the transmitted pulse and the first echo coming through the main beam from the top of the precipitation system detected by the radar (β_n = nadir angle). To increase the sampling rate and thus facilitate the operation of the system as a Doppler radar, it is possible to send radar pulses separated only by the time (approximately 500 μsec) that is required by the radar depth of ground clutter plus the time that is required for atmospheric return, which is a distance of approximately 50 km with the grazing angle discussed here. However, the presence of side lobes may limit this possibility, because there will be additional ground returns occurring from directly below the satellite and beyond (fig. 4–20).

Indeed, at the range at which the atmospheric return is selected, there will also be a contribution from ground clutter "seen" through the side lobes at the same range. The significance of the effect varies with the sea or land backscattering coefficient and the side-lobe level. Preliminary investigations of the clutter problem indicate that the worst effect is due to the near-inside lobe. With a near-inside lobe level of -28 dB or less, 20 to 30 dB of signal-to-clutter ratio can be achieved with 3-mm/hr rain intensity observed over mountains or cities.

If the side-lobe effect can be neglected, a

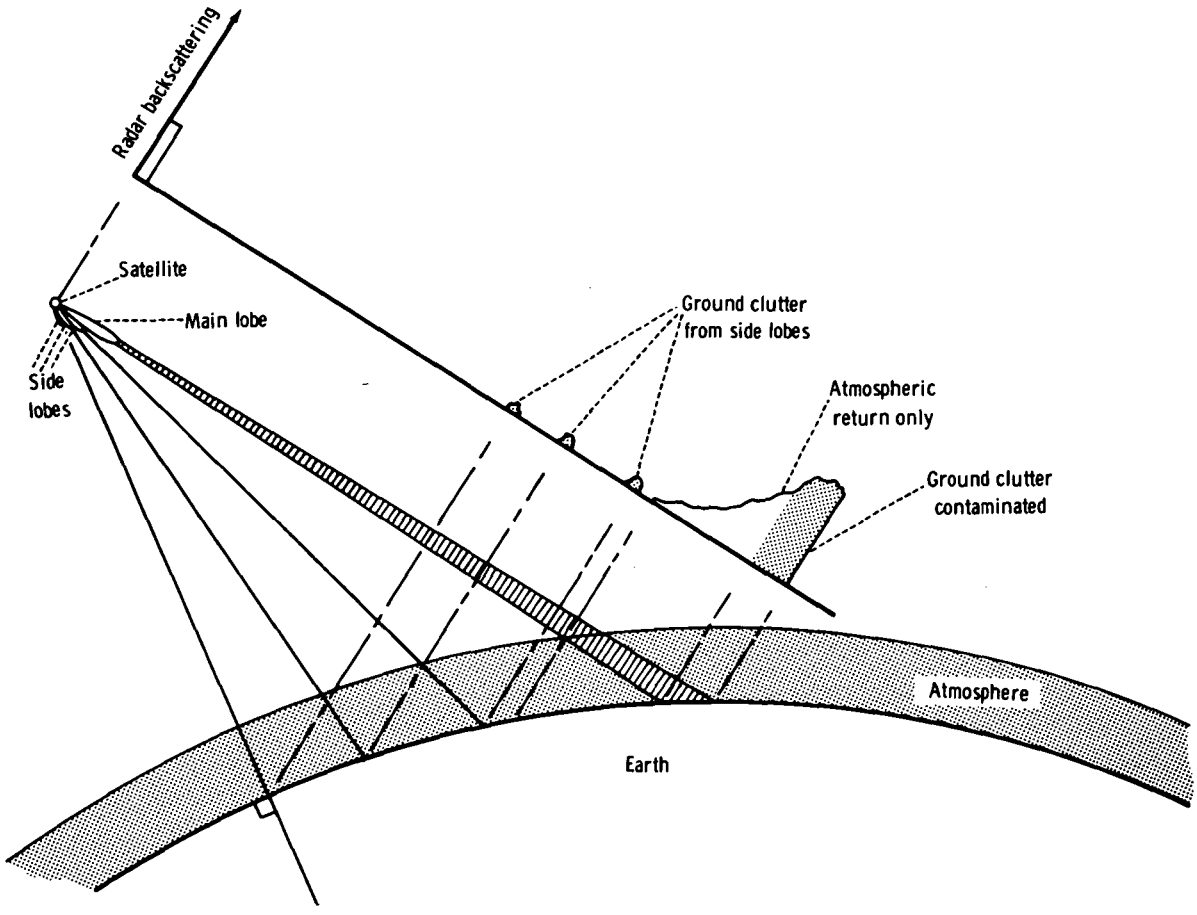

FIGURE 4–20.—Influence of the side lobes in the radiation pattern on the signal received by the satellite radar receiver.

high repetition rate of more than 2 kHz can be used without impairing the range gating of the signal. The critical issue is the selection of atmospheric echoes free of ground-clutter contamination, which implies a range side-lobe level at least greater than 50 dB. Although the discussion here implies a microwave pulse Doppler radar process, other coding methods such as pseudonoise coding can be investigated, as well as the use of a 10-μm radiation provided by a CO_2 laser.

As an example, preliminary investigations show that a 5.6-cm-wavelength pulse radar having the following characteristics

Pulse duration, μsec	10
Receiver bandwidth, MHz	0.2
Antenna effective aperture, cm^2	10^6
Overall noise figure, including losses, dB	10
Peak power, kW	5

provides a signal 15 dB above the receiver noise for precipitation filling the beam at a range of 1000 km and having a reflectivity factor $Z=10^3$.

In the case of the single pencil beam mentioned previously (fig. 4–19(*a*)) (0.3°) and a grazing angle of 20°, the radial size of the beam footprint is 40 km. Because the effective satellite groundspeed is 6.9 km/sec, the scan time per complete revolution as required for full coverage is 6 sec.

There are approximately 1000 different beam positions in each scan, so the time available to sample each position is only 6 msec, which is less than the round-trip time to the targets from the satellite. It is therefore imperative to reduce the scan rate. However, the necessity for full coverage of the swath will require the development of a multibeam capability. A 5- to 10-beam system and an overall scan rate of 40 sec can meet the scan requirements. The beams are contiguous and are used simultaneously with a single transmitter and a single shared receiver. The power required for this type of operation is within current practice.

Considering the echo-free region as mentioned before, the pulse repetition rate can be increased to 2 kHz and still resolve atmospheric and ground targets. Under these conditions, more than 40 samples of the Doppler signal can be available for processing for each beam and range rate.

Neglecting the Earth rotation speed, the Doppler frequency shift V_D due to the satellite velocity is expressed by

$$V_D = V_s \cos\theta \sin\beta_N \qquad (4\text{–}46)$$

where V_s is the satellite velocity, θ is the beam scan angle, and β_N is the beam nadir angle.

In the vertical plane, the spectrum smearing ΔV_D that is due to the satellite motion is mainly controlled by the elevation component of the beam $\Delta\beta_N$, where

$$\Delta V_D \approx V_s \cos\Delta\beta_N \cos\Delta\theta \qquad (4\text{–}47)$$

The Doppler spread in the direction of azimuth scan is expressed by

$$\Delta V_D \approx V_s \sin\Delta\theta \sin\Delta\beta_N \qquad (4\text{–}48)$$

In these expressions $\Delta\beta_N$ and $\Delta\theta$, respectively, are the elevation and azimuth beamwidths, and $\Delta\beta_N=\Delta\theta$ for pencil beam.

The total smearing due to the combined effects is given by

$$\Delta V_D = V_s[(\cos\beta_N \cos\Delta\theta \Delta\beta_N)^2 + (\sin\Delta\beta_N \sin\beta_N \Delta\theta)^2]^{\frac{1}{2}} \qquad (4\text{–}49)$$

With a 0.3° conical beam size, a satellite groundspeed of 7 km/sec, and a grazing angle of 20°, the spectrum smearing due to satellite motion will be approximately 34 m/sec (spectrum standard deviation of $\sigma_v=10$ m/sec) for $\Delta\theta=90°$ and 12 m/sec ($\sigma_v=3.5$ m/sec) in the forward direction.

At C-band and with a sampling rate (pulse repetition rate) of 2 kHz, the mean of spectra with a width smaller than 50 m/sec can still be processed by use of optimum estimators, such as the covariance estimator mentioned in the section entitled "Doppler Radar Signal Processing."

It can be shown that, with a signal dwell time of 0.05 sec (time during which the beam rotates by one beamwidth for a total conical scan time of 50 sec) and a spectrum standard deviation of 10 m/sec, the standard deviation

σ_v of the mean Doppler estimate is approximately 2 m/sec.

For a satellite groundspeed of $V_s = 7.0$ km/sec and $\beta_N = 60°$, $V_D \approx 6$ km/sec in the forward direction. At C-band, this is equivalent to a Doppler frequency shift of approximately 200 kHz. Assuming a sampling rate of 2 kHz will place the spectrum in the 100th frequency ambiguity region. However, the satellite groundspeed is extremely stable, and the sampling rate can also be easily made very stable and accurate. Various schemes are available to reduce the velocity ambiguity problems. It may be possible, for example, to use the ground Doppler shift as a reference. The range-gated ground return is expected to occupy a well-defined mean frequency position, which can be used as a reference, thereby allowing the unambiguous resolution of the groundspeed of atmospheric targets.

The continuous change of the scan angle during the beam rotation, combined with the satellite groundspeed, produces continuous variations of the mean Doppler frequency shift and spectrum smearing. If the radar is equipped with onboard processing systems capable of tracking spectrum mean frequency at four or five range gates in the atmospheric region and one in the ground clutter, this information can be continuously transmitted to Earth with low-bandwidth systems also telemetering scan angle and satellite position. The processing of this information by a ground-based computer can provide estimates of quasi-horizontal velocity in regions where atmospheric targets are "seen" from different angles during the satellite motion.

Table 4–VI outlines tentative specifications for such a satellite system. The critical part of these specifications is the maximum PRF that can be used. In the case of a radiation pattern free of side lobes and with the grazing angle of 20°, the minimum time between successive pulses is 400 to 500 μsec. This repetition rate of 2 kHz, which places the forward Doppler in the 100th ambiguity region, should still allow discrimination between atmospheric and ground-clutter speed with 35-m/sec-or-less Doppler smearing. Signal covariance estimators or equivalent are needed for accurate tracking of spectral mean.

TABLE 4–VI.—*Tentative Specifications for a Multibeam Doppler System*

Radar wavelength, cm	5.6
Peak power (per beam), kW	5
Average power, W	100
PRF (stability better than 10^{-4}), kHz	2.5
Pulse width, μsec	10
Antenna beamwidth, deg	0.3
Beam footprint on the ground, km	5 by 15
Beam nadir angle, deg	60
Grazing angle, deg	20
Conical scan, beam scan time, sec	40
Satellite displacement during complete scan, km	280
Angular displacement of the antenna beam during echo round trip, deg	0.13
Satellite orbit	polar inclined
Satellite altitude, km	≈500
Satellite orbit time, hr	1.6
Satellite groundspeed, km/sec	≈7
Forward-groundspeed Doppler shift, kHz	≈200
6-dB Doppler smearing (max), m/sec	35
Nonambiguous velocity interval, m/sec	70

This first example is an attempt to describe a possible specific solution for a low-orbit satellite-borne weather radar capable of a coverage comparable to that obtained with orbiting satellites now used in meteorology. The radar is primarily a conventional radar and could serve as a reference for further discussion and development. The choice of the wavelength implies the availability of large antennas, such as the one recently flown with ATS–F. The technology of large dish antennas to be used aboard satellites will certainly improve in the next few years, but for the present it appears that geostationary satellites are reserved for imagery done in the infrared or visible part of the spectrum, for which well-collimated beams are easy to obtain.

In summary, if the radar method is restricted to low-altitude orbiting satellites for

which the groundspeed is large, then the application of Doppler techniques will be very difficult, but not impossible. Also, low-altitude orbiting satellites require the use of beam scanning techniques that produce a swath of sufficient dimension so that complete coverage from orbit to orbit is obtained. A conical scanning method, which is easy to obtain simply from the spinning of the satellite, has been presented. This scanning method also allows the same point on Earth to be probed from a different direction during the satellite motion, therefore offering some possibilities of resolving quasi-horizontal velocity.

The design and implementation of such methods must be preceded by a thorough feasibility study. The purpose of the example presented earlier is to focus the discussion on a specific system for which such a feasibility study can be done.

In addition to the measurement of precipitation, the most significant contribution that active microwaves may make to atmospheric measurements is to observe the windfield inside precipitation systems. Ideally, the meteorologist would like to have synoptic maps of windfields at several altitudes and, under certain conditions, measured as frequently as several times an hour. Such global-scale maps would improve forecasting and would also allow accurate assessment of global atmospheric motion. When used in conjunction with the passive optical satellites, the maps would permit the identification of precipitating clouds and the assessment of their severity.

The Doppler wind-measurement method presented here is a unique capability available only to active microwave systems and only requires that the detectable tracers have no motion relative to the winds. Naturally, the active technique permits the measurements to be made on both the light and dark parts of the orbit.

The microwave Doppler weather measurements rely on basically the same backscattering phenomenon as the conventional radar. The unique aspect of the measurement is that the method is sensitive to the motion of each of the particular scatterers.

Preliminary study indicates that current state-of-the-art equipment can provide useful Doppler measurements. The system recommended in this section uses a conical scan obtained by rotating a tilted pencil-beam antenna. A low-altitude orbit (500 km) is used to reduce the required antenna dimension. The radar frequency would lie in the C- to X-band region. The coverage provided by a single satellite is sufficient to guarantee at least two passages a day over the global region between $\pm 70°$ latitude. The scanning pattern provides two observations for each pass over more than 70 percent of the swath, with sufficient angular diversity to obtain representative wind magnitude and direction. Accuracy of approximately 2 m/sec is available for each measurement. Altitude resolutions of 5 km (two-way 3-dB points) are available with current technology and may be improved in the future. The principal limitation is ground clutter, which requires a narrow-beam ($<0.3°$) antenna.

The scanning technique produces a swath with a width in excess of 2000 km. Availability of two-dimensional windfields would provide a snapshot of the entire windfield of a tropical-storm system such as a hurricane. If the storm were at a higher latitude (20°), two or more such snapshots spaced by 1.6 hr would be obtained.

The instrument needed in an advanced system would require an approximately parabolic 11-m antenna, a 1-kW peak-power transmitter operating at C-band, a low-compression coded waveform (1 MHz, time bandwidth <100), and an onboard system that processes reflectivity and mean Doppler speed.

Available technology indicates that the electrical equipment, exclusive of the solar cells but including the antenna and signal processor, might have a total weight of less than 500 kg. Data reduction on board the satellite would reduce the downlink average data rate to 4×10^5 (5-bit) samples/sec, even with no data editing. On the ground, cor-

rections for the satellite orbit and the attitude errors would be inserted. Even with communications delays, initial systems should be able to achieve 24-hr timeliness, with future systems achieving satellite sampling-time timeliness by the use of geosynchronous satellite communication systems.

The first priority is a thorough feasibility study to determine optimum parameters. Next, an experimental study should demonstrate the measurement principles and carry out the data reduction. Early experimental models should then be tested on existing platforms. The meteorological significance of these preliminary results should be reassessed; and, finally, a full-scale system should be planned and executed.

Geosynchronous Satellite

The geometry of a geosynchronous satellite is shown in figure 4–21. Assuming a convective precipitation cell at a great circle distance L from nadir, the expected radar echoes, if detectable, would probably have a time/distance dependence similar to that sketched in figure 4–21. The round-trip time delay τ_0 is approximately 0.25 sec, and the ground return is expected to be significantly higher than the return from precipitation. However, at shorter wavelengths (i.e., 10 μm), regions of precipitation could be masked by cloud cover. If $\tau_n < \tau_0$, where τ_n is the time delay for ground echoes detected at 0° nadir angle, no side lobes or main beam intersect the Earth; and the distance L to which precipitation targets alone are detected to height h (and delay τ_n) is given by the approximate expression

$$L = \frac{\sqrt{2hR_s}}{1+\frac{R_s}{R_E}} \qquad (4\text{–}50)$$

This expression indicates, for example, that if the measurement of vertical motion at a constant 10-km height is required, clutter-free observations can be made to distances L of approximately 330 km from nadir. Although a 700-km-diameter area may be sufficient to observe motion along a particular

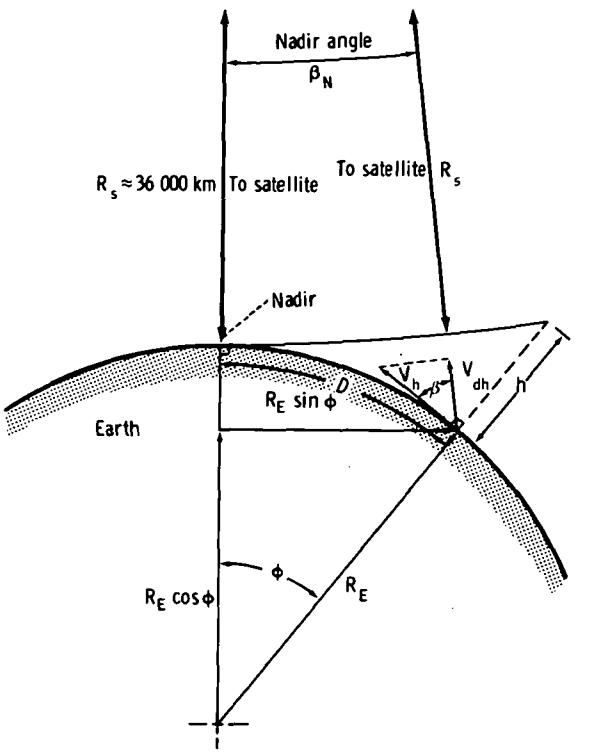

FIGURE 4–21.—Geometry of a satellite in a geosynchronous orbit.

entire squall line (for $h \geq 10$ km), it is too small to cover the vast area over which squall lines can form and would be restricted to equatorial regions. A ground-based radar can make observations over a diameter of 400 km; therefore, no great advantage in area surveyed would be derived from the use of a geostationary satellite radar for vertical velocity measurements.

It must be noted that the distance L from nadir, for which accurate vertical velocity measurements can be made, is also limited by the presence of the projection V_{dh} of velocity V_h on the radar radial direction. For small nadir angle β_N,

$$\frac{V_{dh}}{V_h} = \cos\beta \approx \left(\frac{1}{R_E}+\frac{1}{R_s}\right)L = \left(1.88\times10^{-4}\right)L \qquad (4\text{–}51)$$

where L is in kilometers. The contribution to radial velocity due to a 30-m/sec horizontal motion, for example, is 1.6 m/sec at

300 km from nadir. Therefore, to keep vertical velocity contamination below 2 m/sec, L must be less than 350 km, which limits the area of surveillance of vertical wind to a 700-km-diameter circular region.

The solution involving the use of a satellite in a high-altitude (36 000 km) geostationary orbit requires the availability of an extremely narrow beam. Because the radiating antenna size is limited, such a narrow beam can only be obtained with a very short wavelength. However, operation near vertical incidence involves less strict range ambiguity considerations, and wavelengths as small as 1 cm may be used. For example, if a 10-m dish, such as the one recently flown with ATS–F, could be used at 1-cm wavelengths, a beamwidth of approximately 0.06° with a beam footprint of approximately 45 km on the Earth surface would be obtained. This resolution is much poorer than the resolution (a few kilometers) provided by infrared and visible sensors installed aboard geostationary satellites such as ATS–3 and GOES, but it could still provide information on large-scale systems.

In addition, the use of such a short wavelength will be associated with prohibitive absorption of the radar signals (approximately 10 dB/km two ways, for a 25-mm/hr precipitation), so that penetration of the storm and quantitative observations would be questionable.

It can be concluded that, even if radar antennas (space qualified at 1-cm wavelength) can ultimately reach a 10- to 20-m size, the operation of 1-cm microwave radar aboard a geostationary satellite will still be highly questionable. The problem may be overcome only by substituting a CO_2 laser-type system operating at 10 μm, which might offer a more appropriate solution for geostationary satellite operation. At least, this system meets the resolution requirements, although coverage is still restricted to equatorial regions.

Carbon Dioxide Pulsed CW Doppler Radar

The purpose of this section is to determine whether mesoscale information can be derived from a 10-μm Doppler radar in synchronous orbit. In particular, an attempt is made to answer the question, "Can organized vertical motion of precipitating regions be resolved?"

The objective is to determine the parameters required for a 10.6-μm radar to detect and resolve the vertical velocity in a precipitation cell 2 km in diameter. A quantum-limited detector is assumed when the receiver noise power is (ref. 4–57)

$$P_N = B\left(\frac{h_1 c}{\eta\lambda} + kT_a\right) \qquad (4\text{–}52)$$

where

B = bandwidth $= 0.7/\tau_p$ (where τ_p is dwell time $= 2\Delta h/c$)
$T_a = 300$ K
k = Boltzmann constant, 1.38×10^{-23} J/K
η = quantum efficiency of detector = 80 percent
h_1 = Planck constant, 6.6×10^{-34} J-sec

Substituting these values into equation (4–52) yields

$$P_n = \frac{1.05\times10^{8}}{\Delta h}(2.48+0.414)\times10^{-20} = \frac{3\times10^{-12}}{\Delta h} \qquad (4\text{–}53)$$

where Δh is in meters. The precipitation backscatter cross section per unit volume σ_v as compared with reflectivity factor Z is plotted in figure 4–22 for $\lambda = 10.6$ μm. Transmitted peak power in excess of 1 MW would be required to detect a 30-dBZ precipitation cell of 2-km diameter with a 2-km vertical resolution, even if absorption is neglected. Although detection of precipitation is impractical, clouds have scatter cross sections that are orders of magnitude larger than precipitation; hence, cloud boundaries may be detected from geostationary altitudes. Further work along this direction may be required if significant meteorological information can be derived from cloud vertical velocities viewed over limited (several hundred kilometers) equatorial regions.

Reducing the satellite orbiting altitude to a lower value (e.g., 400 km) will result in considerable sensitivity gain (40 dB) if the

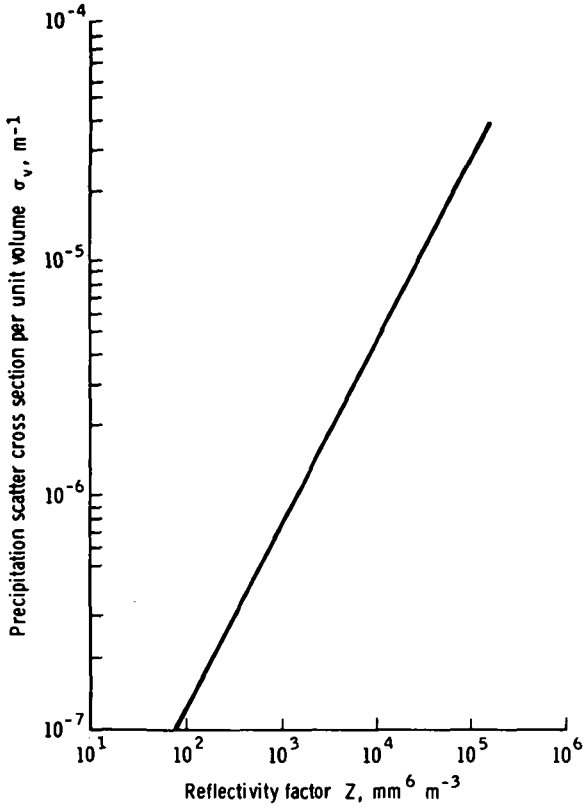

FIGURE 4–22.—Precipitation backscatter cross section per unit volume σ_v compared with reflectivity factor Z for $\lambda = 10.6$ μm.

other parameters are fixed. Therefore, thin clouds of lower water content can be used as tracers of air motion. Rensch and Long (ref. 4–58) made theoretical computations concerning fog scattering and attenuation. The authors show that, for $\lambda = 10.6$ μm and the droplet radius for maximum number density $a_m = 1$ μm, σ_v is approximately 3×10^{-7} m^{-1}/mg m^{-3}. Thus, for water clouds with water content of 10^3 mg m^{-3} which is appropriate for cumulus clouds, σ_v is 3×10^{-4} m^{-1}, which is an order of magnitude larger than the return from precipitation. This discussion does not provide a comprehensive treatment, but it does illustrate that the CO_2 Doppler laser has definite advantages in sensitivity and resolution for measurements of cloud motion, although it cannot penetrate thick cloud regions. Furthermore, returns from particulate matter for satellite-borne lasers ($\lambda =$ 0.7 μm) have been theoretically demonstrated to be possible (ref. 4–59). Investigations concerning CO_2 scatter cross section from in situ atmospheric aerosols and the spatial distribution and density of these aerosols should be vigorously pursued to determine the feasibility of clear-air detection of atmospheric motion from satellites. Although the CO_2 laser will not penetrate heavy cloud systems, the ability to detect and resolve speed and location of cloud particles may constitute an attractive alternative to a 6-cm microwave system.

Absorption of 10.6-μm radiation by water vapor for the entire atmosphere at normal incidence is less than 2 dB (ref. 4–60). Absorption of CO_2 laser radiation due to atmospheric airborne dioxide has also been computed. The total two-way absorption is less than 6 dB. Rain scatter and absorption losses have been computed by Rensch and Long (ref. 4–58), who have assumed a Gaussian distribution of drop size fitted to the tabulated size distribution of Laws and Parsons. By far, the largest attenuation is associated with propagation through cloud. Theoretical computations on fog attenuation, assuming a cloud droplet-size distribution of the form

$$N(a) = C\left(\frac{a}{a_m}\right)^6 e^{-6(a/a_m)} \qquad (4\text{–}54)$$

(where C is a constant and a_m is the droplet radius for maximum number density), show a 10.6-μm total attenuation normalized to liquid water density of approximately 1.5×10^{-1} dB/km/mg m^{-3} for mean drop radii between 20 and 10 μm. Larger droplet diameters produce decreasing attenuation for constant water content. Liquid-water concentration in cumulus clouds may be several g/m^3, and thus the attenuation rate due to cloud droplets may exceed 100 dB/km, overwhelming the absorption due to precipitation itself. The experiments of Chu and Hogg (ref. 4–61) of CO_2 attenuation verified that fog attenuates considerably more than raindrops.

Considering all the possible loss mechanisms, it appears that a CO_2 laser will, at

best, be able to measure only the motions of cloud boundaries.

Doppler radar measurements at a 10-μm wavelength may be attractive for several reasons. Calculation shows that detection of cloud particles is feasible from an orbiting satellite. Surveillance of larger areas of atmospheric motion than that achieved with microwave radar may improve because microwave radar is limited to detection of precipitation regions. A 10-μm-wavelength Doppler radar has range and velocity information contained in a single pulse of several microseconds' duration, resulting in mean velocity information being acquired at a rate much faster than that possible with a microwave system.

The measurement of cloud motion with a CO_2 Doppler radar may have an advantage over present techniques of mapping cloud positions photographed from geostationary satellites, because the radar can resolve cloud height. Although the radar measures only radial velocities, the measurement of air motion from two directions is possible so that vector wind direction can be achieved. The use of a CO_2 laser aboard a satellite may have an advantage over ground observations, because turbulence degradation of coherency should not be as severe when looking at clouds from above.

Vertical motion from geostationary satellites appears to be limited to observations of cloud tops. Vertical motion measurements will be constrained by the location of the geostationary satellite to regions near the equator.

APPLICATIONS OF BISTATIC MICROWAVE SYSTEMS TO ATMOSPHERIC RESEARCH

An active microwave system is one that incorporates both a transmitter and a receiver. In the situation most commonly considered, both the transmitter and receiver are in the same place; they are often in the same cabinet or in the same vehicle, or at least in sufficient proximity to permit the same operators to attend to both devices. This arrangement of equipment is called "monostatic." When the microwave transmitter and receiver are distant from one another, the system is termed "bistatic." The actual separation distance required to permit a choice between these two descriptive terms has not been agreed upon, but generally the bistatic name is applied to any system for which the analysis of the radar return requires consideration of the separation.

Bistatic radar systems have been used very effectively in applications as diverse as planetary astronomy observations and lunar surface soundings by orbiting spacecraft. It is therefore very likely that the bistatic techniques developed during the last decade will be used to considerable advantage in future active microwave applications.

The separation of transmitter from receiver often leads to inherent advantages, and one of these advantages usually accounts for the choice of a bistatic system in any given application.

In some circumstances, one wishes to measure the behavior of microwave propagation along a particular radio path. If the transmitter and receiver are at opposite ends of the path, the signal has to traverse the path in only one direction, and the loss is only one-way instead of two-way, as in the conventional monostatic radar case. Therefore, for path sounding, the bistatic approach may lead to a much lower requirement for signal strength and reception capability because of the decrease in the total loss of the system.

When the transmitter and receiver are close together, the receiver must be designed so that it can operate with the interference that inevitably results because of the presence of the nearby transmitter. By separating the transmitter and receiver, these problems are usually eliminated, or at least alleviated. The result is that comparatively simple modulations can be used; in fact, CW modulation becomes practical, and other quasi-continuous modulations may also be readily accommodated. This generally leads to a simplification of the hardware and, therefore, a decrease in cost, provided, of course, that

the objective of the system can be met with the bistatic configuration.

Many kinds of radio-wave scatterers do not produce a large backscatter return, although they may scatter a very large amount of energy through small angles. If a microwave transmitter is directed at such a body of scatterers and the receiver shares the same antenna, it will obtain a small return. A similar receiver located behind the scatterers and just off the transmitter-scatterer axis would receive a relatively strong return. It is sometimes possible to configure a bistatic radar system to take advantage of this effect, whereby small scattering angles lead to a large radar cross section.

In some circumstances, it is helpful to have a variable scattering angle to permit the measurement of radar cross-section variation with respect to the scattering angle. In the case of the lunar bistatic scattering experiment, the variation of the cross section with respect to angle permitted an inference of the Brewster angle, from which the dielectric constant of the lunar surface could be determined independently of the scattering model adopted by the observer. The measurement of the dielectric constant by direct return is comparatively inaccurate.

In some circumstances where the radio path from transmitter to receiver is almost straight and the signal is rather stable, the polarization of the signal can be controlled; therefore, its polarization changes can be observed with a high degree of accuracy. This may permit polarization analyses that would be impractical with a monostatic system.

Strictly speaking, one-way transmission experiments fall into the bistatic active microwave system category. Systems of this type operating in the millimeter-wavelength region are often the best suited for fundamental studies of the gaseous constituents of the atmosphere and the forward-scattering properties of hydrometeors. It is likely that, in the area of transmission experiments, bistatic techniques will be used for atmospheric problems in the next few years. For many meteorological and atmospheric physics studies, it is important to know the size, composition, shape, and orientation of hydrometeors. The best experimental approach to determining these parameters is to transmit a known polarization (linear or circular) from a satellite to a ground antenna that is instrumented to carry out a precise polarization analysis of the scattered signal. Such studies are of considerable importance to theoretical modeling of the scattering of microwaves by an assembly of nonspherical hydrometeors. In addition to the obvious importance to atmospheric physics, the results are of crucial importance to advanced satellite communications work.

The rationale for current satellite communication experiments is the lack of available channels in the frequency range below 10 GHz, where atmospheric effects are relatively unimportant. Above 10 GHz, microwave radiation interacts strongly with raindrops and ice particles, and measurements of attenuation and depolarization are planned or in progress to characterize these interactions. The goals of these experiments are primarily to gather statistical data and advanced communications technology, but meteorological information can and should be gathered as well.

After a series of investigations of 10- to 30-GHz attenuation and depolarization, theoretical models for propagation through rain were developed for terrestrial paths. These models involve the size and shape distributions of the raindrops and provide insight into the relationship between these distributions and observed attenuation and depolarization. The distributions generally accepted for ground rainfall are of questionable validity at high altitudes. In addition, Earth-satellite paths must penetrate the melting layer, and little is known about the ice-particle size and shape distribution in this layer. The planned propagation experiments will provide new information concerning both of these distributions.

An additional consideration is the possible depolarization by ice crystals in cirrus clouds. This effect may be important to meteorology. The available information is insufficient to

support a quantitative prediction; but qualitatively, if the ice crystals show some degree of alinement, it should be possible to calculate their size and number by measuring their depolarizing effects at two frequencies using linear polarization. If ice-crystal orientation is random, their effects in circular polarization may be a good indication of their number and composition.

The high degree of stability of the background signal can be used to allow accurate studies of gaseous atmospheric constituents. The scintillations in the signal, if detectable, would provide a clue to the observation of atmospheric turbulence. Heavy precipitation should be detectable by this means if the signal is stable and well calibrated in amplitude. The total water content could be determined by observing and measuring signal absorption. It might be possible to measure the vertical distribution of a constituent by taking advantage of the pressure broadening of its absorption lines, using a forward-propagated signal at multiple wavelengths. One might even sweep the transmitted signal frequency across an absorption band to provide a complete frequency sample of the shape of the band of some particular molecule of interest. By choosing different absorption bands that are characteristic of different constituents, one could measure the specific atmospheric constituents individually.

PART B

ADDITIONAL APPLICATIONS AND RELATED TOPICS

THE MEASUREMENT OF SURFACE PRESSURE FROM A SATELLITE BY ACTIVE MICROWAVE TECHNIQUES

Although it is now possible to map the temperature structure of the atmosphere from satellites, pressure measurements are still limited by the coverage of ground-based instruments. More data are required from wider areas as an input to long-period numerical forecasts. Satellite methods for pressure measurement should be investigated. The following data requirements for a set of global meteorological measurements sufficiently accurate to provide initial conditions for a numerical forecast up to 2 or 3 weeks ahead have been specified by GARP (ref. 4–62):

1. Wind components: ± 3 m/sec
2. Temperature: ± 1 K
3. Pressure of reference level: ± 0.3 percent
4. Water vapor pressure: ± 100 N/m^2
5. Time average interval: 2 hr
6. Horizontal space average: 100 km
7. Vertical space average: eight levels at 100 000, 90 000, 70 000, 50 000, 20 000, 10 000, 5000, and 1000 N/m^2, respectively.

Such a vast amount of data can possibly be collected in the necessary time and at a reasonable cost only by the use of remote-sounding instruments on satellites. Although a geostationary satellite provides the most convenient platform for such closely spaced observations, it has the disadvantage of being at a very large distance (36 000 km), so that the antenna size required to achieve an acceptable ground resolution or to intercept sufficient energy of a return echo may be prohibitive. Therefore, for the purpose of this discussion, it is assumed that the instrument is mounted on a satellite orbiting at approximately 1000 km.

An accuracy of ± 0.3 percent in a pressure measurement corresponds to a height change of only 20 m, so that the height at which the pressure is measured must be known to within this value. This requirement renders the measurement of the three-dimensional pressure field very difficult. In principle, the desired accuracy might be achieved by a radar or lidar technique, but any pressure-